Recent advances in thermophysical properties enhancement of phase change materials for thermal energy storage

Karunesh Kant, Pascal Henry Biwole, I. Shamseddine, G. Tlaiji, F. Pennec, F. Fardoun

Recent advances in thermophysical properties enhancement of phase change materials for thermal energy storage

K. Kant[a,b,*], P. H. Biwole [a, c], I. Shamseddine [a, d], G. Tlaiji[a], F. Pennec[a], F. Fardoun [d,e]

[a] Université Clermont Auvergne, CNRS, Clermont Auvergne INP, Institut Pascal, F-63000 Clermont-Ferrand, France

[b] Advanced Materials and Technologies Laboratory, Department of Mechanical Engineering, Virginia Tech, Blacksburg, VA 24061-0238, USA

[c] MINES Paris Tech, PSL Research University, PERSEE - Center for Processes, Renewable Energies and Energy Systems, CS 10207, 06904 Sophia Antipolis, France

[d] Université Libanaise, Centre de Modélisation, Ecole Doctorale des Sciences et Technologie, Hadath, Liban

[e] Faculty of Technology, Department GIM, Lebanese University, Saida, Lebanon

*Corresponding Author- k1091kant@gmail.com

Abstract

Phase change materials (PCM) are promising technology to store thermal energy at a constant temperature. A large amount of energy can be stored or released in latent heat form during the transition of material from one phase to another. Despite the great benefits, most PCMs have their own limitations i.e., low phase change enthalpy, poor specific heat and thermal conductivity, supercooling, volume change, phase segregation, etc. Consequently, efficient thermal energy storage requires improving the thermophysical properties of PCMs. The present study is a comprehensive review of existing techniques for PCMs thermophysical properties enhancement. The research progresses on adding zero, one, two, and three-dimensionally structured additives to PCM is assessed to improve the thermal transport by enhancing the PCM effective thermal conductivity. The enhancement of latent heat of fusion and specific heat using various additives is also discussed. Further, the latest techniques on supercooling and phase segregation reduction are also presented. Last, the modelling of the novel composite materials formed by combining a PCM with other materials is presented. Despite the fact that the majority of these methods are still in the research and development stage, some of them have the potential to be commercialized in the near future. Reliable and efficient PCMs are exceptionally useful for storing solar energy and industrial waste heat, especially for constant temperature applications.

Keywords: PCM; Thermo-physical properties enhancement; composite PCM; Thermal energy storage; Supercooling

1. Introduction

The demand for energy and its utilization is increasing rapidly due to population growth and improved living standards [1–3]. The supply of energy still mainly depends on traditional energy sources such as coal and fossil fuel. However, traditional energy sources have several disadvantages such as their unbalanced geographical distribution in the different countries, which increases investment costs in transport and security for countries with low resources, and their direct impact on the environment signified by global warming and its impacts on the ecosystem. Moreover, these resources are limited and severe consumption leads to its unavoidable deficiency [3]. To overcome the above-mentioned challenges, the need for clean, cheap, and sustainable energy sources becomes a priority. The use of renewable energy sources (solar, wind, and hydro, etc.) decreases the demand for traditional resources of energy and serves in decentralizing the energy supply. Renewable energy sources are abundantly available, however intermittent in nature [4]. For example, the productivity of photovoltaic panels depends on the presence of light, which in turn is dependent on time and season (day or night, position of the sun). Due to intermittency in the energy supply, energy storage devices are required to reduce the gap between energy demand and supply. The energy storage systems store excess energy to be used later in deficiency periods. Phase change materials (PCM) are materials that can store solar thermal energy to enhance the performance of solar thermal systems. PCM change phase at a constant temperature by absorbing or releasing heat energy in the form of latent heat. PCM can be utilized for several applications such as concentrating solar power (CSP) plants [5], thermal management of photovoltaic [6,7], buildings [8], electronics cooling [9], etc. However, the thermophysical properties of PCM are responsible for several limitations. These limitations are associated with the PCM's ability to store and transport heat. In other words, the behavior of any PCM depends on its thermophysical properties such as thermal conductivity, heat capacity, latent heat, degree of supercooling, phase segregation, etc. The low thermal conductivity imposes a prolonged time to release and store the thermal energy, which reduces the performance of the energy storage device. The low specific heat and latent heat of fusion result in a larger volume of the thermal energy storage device to store the thermal energy. Supercooling may delay the start of thermal energy release while phase segregation may eventually lead to material degradation. These phenomena are undesired and may dramatically change the behavior of the system by causing severe problems to its efficiency.

During the past decade, significant efforts have been made to improve the properties of the PCM in order to make them more efficient and cost-effective. The current study delves into the specific methods for improving PCM thermophysical properties. Despite the fact that the majority of these methods are only in the research and development stage, some of them have the potential to be commercialized in the near future. In the first part of this paper, thermal energy storage using PCM is described. Next, a detailed discussion on enhancing thermal conductivity, latent heat of fusion, and specific heat capacity by different methods is presented. The following section presents the main reasons that cause supercooling and phase segregation as well as the applied techniques to suppress these phenomena. Further, the different modeling techniques to model the newly developed composite PCM are outlined. Finally, future developments are discussed.

2. Thermal energy storage using PCM

Thermal energy storage using PCM is based on the heat absorption or release when a storage material undergoes a reversible phase change from solid to liquid, liquid to gas, solid to gas, solid to gas, or solid to solid, as shown in Figure 1 [10]. The most commonly used latent heat storage systems undergo solid-liquid phase transitions due to large heat storage capacity and small volume change between phases [11,12]. When the temperature exceeds a certain threshold (i.e., the phase transition temperature), solid-liquid PCMs shift their internal molecular arrangement from an ordered crystalline structure to a disordered amorphous form. An increase in vibrational energy breaks the supramolecular connections that hold individual molecules together, causing the crystalline arrangement to degrade into a randomly oriented liquid state (Figure 2) [13]. In reverse, when temperatures fall below the phase transition temperature, a nucleation process begins, in which molecules reorganize into a crystalline lattice. Many factors influence the shape and number of crystals that form during crystallization, including cooling rate, molecule type, and the presence of impurities that can act as nucleating agents. The advantages offered by solid-liquid PCMs lead to their contribution in different applications such as greenhouses [14–16], photovoltaic systems [17–19], buildings [20–23], cooling systems [24], heat sinks [25–27], and other applications.

The solid-liquid phase changes are accompanied by a volume change, with volume typically increases when the material becomes liquid. Organic PCMs (e.g., paraffin) and inorganic PCMs (e.g., salt hydrates), as well as various mixtures of these (e.g., eutectics), are common solid-liquid PCMs utilized for thermal energy storage [28]. Various strategies can be used to

enhance the performance of solid-liquid PCMs for thermal storage applications by addressing their inherent drawbacks. For example, the phase transition temperature of paraffin can be tailored by changing the length of the carbohydrate chain. The low thermal conductivity of most solid-liquid PCMs is among the main barriers for many thermal energy storage (TES) applications [29] because of the reduced heat transfer rate. Some other practical challenges of using solid-liquid PCMs include the need for containment or encapsulation when in the liquid state to avoid leakage, the occurrence of phase segregation in mixed systems when going through multiple phase change cycles, material degradation, supercooling, and hysteresis occurring between cooling and heating cycles. The following paragraphs discuss the enhancement of PCM thermophysical properties, to increase the performance of thermal storage systems.

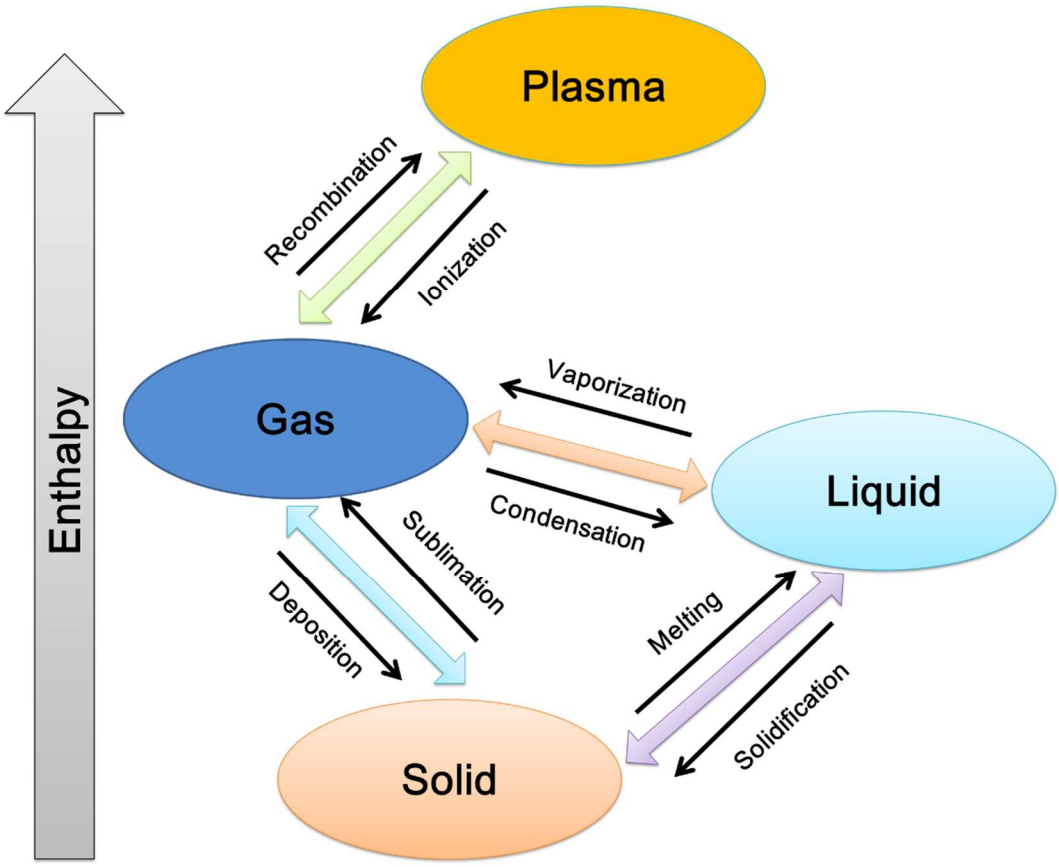

Figure 1 Possible phase transitions of materials [10]

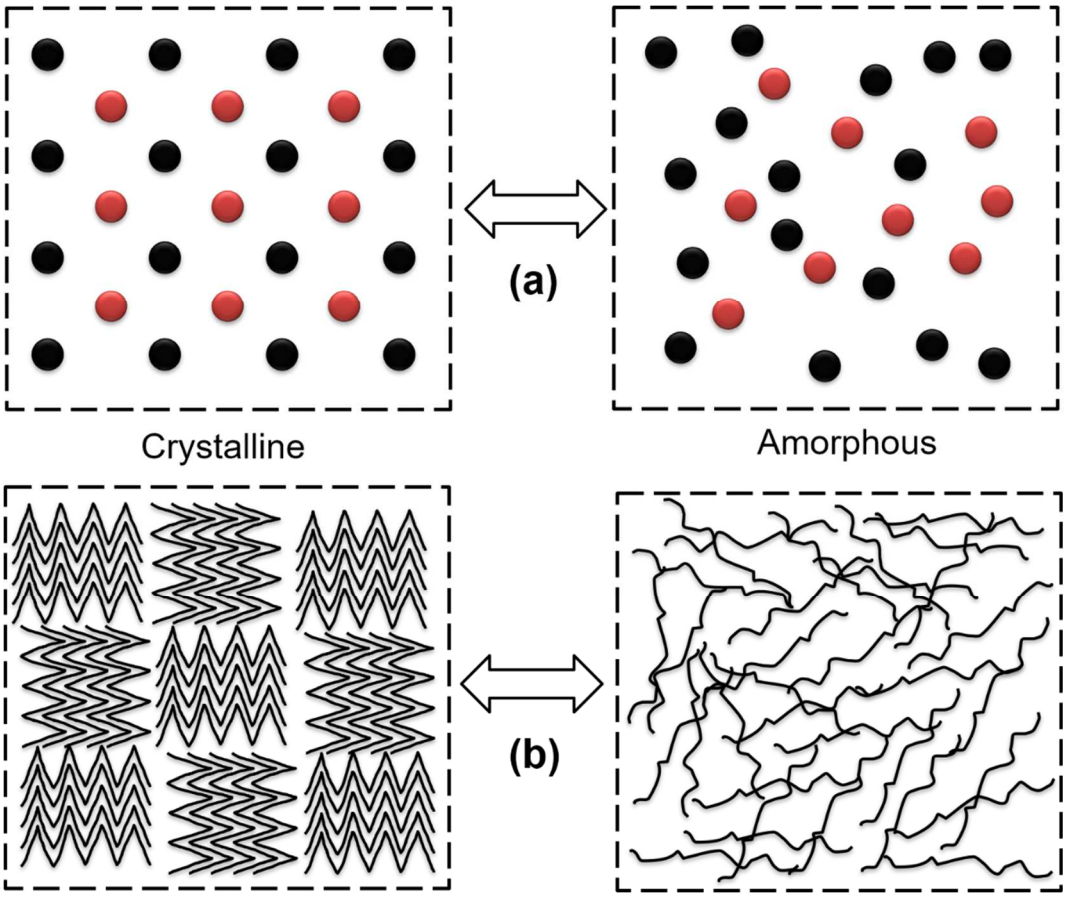

Figure 2 Schematic representation of solid-liquid PCM's phase change processes for (a) A salt-hydrate system transitioning from an ordered crystalline to a disordered non-crystalline phase, and (b) transition of a paraffin-type system from a lamellar crystal phase to a random disordered phase [13].

3. Enhancement of thermal conductivity

One of the main issues for PCM in latent heat storage applications is thermal conductivity enhancement. Several theoretical and practical investigations were conducted to examine the heat transmission process of various latent heat storage systems [30]. Currently, the major ways for increasing the thermal conductivity of PCM are to add a high thermal conductivity matrix and chemically modify the additive's surface. These include surface and grafted functional group modification, as well as the inclusion of porous three-dimensional (3D), two-dimensional (2D), one-dimensional (1D), and zero-dimensional (0D) structural additives. Although modification and grafted functional groups can increase material compatibility and reduce interfacial heat resistance, the success rate of modification is lower and the operation is more intricate. The inclusion of a thermal conduction matrix can result in the formation of a thermally conductive chain, which reduces phonon scattering and speeds up heat transmission. Higher additive mass content, on the other hand, will considerably limit PCM's heat storage capability. As a result, while selecting techniques to increase the thermal conductivity of PCM, the appropriate additional amount and experimental conditions should be taken into account.

3.1. Mechanism of thermal conductivity

The low thermal conductivity of PCMs is a major drawback. The development of composite materials with high thermal conductivity matrices can solve this problem. Thermal conductivity enhancement of PCMs using composites is still a prominent research subject [28,31–35]. A variety of factors influence the thermal conductivity of PCMs, and phonon scattering is one of the most important factors that limit the thermal conductivity of composite PCMs. The phonon is the most fundamental description of thermal transfer at the microscopic level, as well as a moving force that transports heat from one end to the other. The factors that govern phonon transmission in composites are basic heat power, phonon velocity, and mean free path. Heat transport in PCM and interfacial phonons are not constrained to each of these parameters since they are influenced directly or indirectly by a number of other factors such as atomic weight, temperature, mass, and binding energy. Various studies have discussed heat transmission in the materials by lattice vibration and phonon transmission [34–39].

3.2. Methods to increase PCM thermal conductivity

By analyzing the microscopic structure of the materials, the thermal conductivity of the PCM can be enhanced. The heat transfer mechanism is affected by the morphological structure of the PCM. Figure 3 depicts various pathways for improving a PCM thermal conductivity. This section presents PCM thermal conductivity enhancement by chemical modification, as well as the morphological characterization, preparation methods, and microscopic level description of composite PCM.

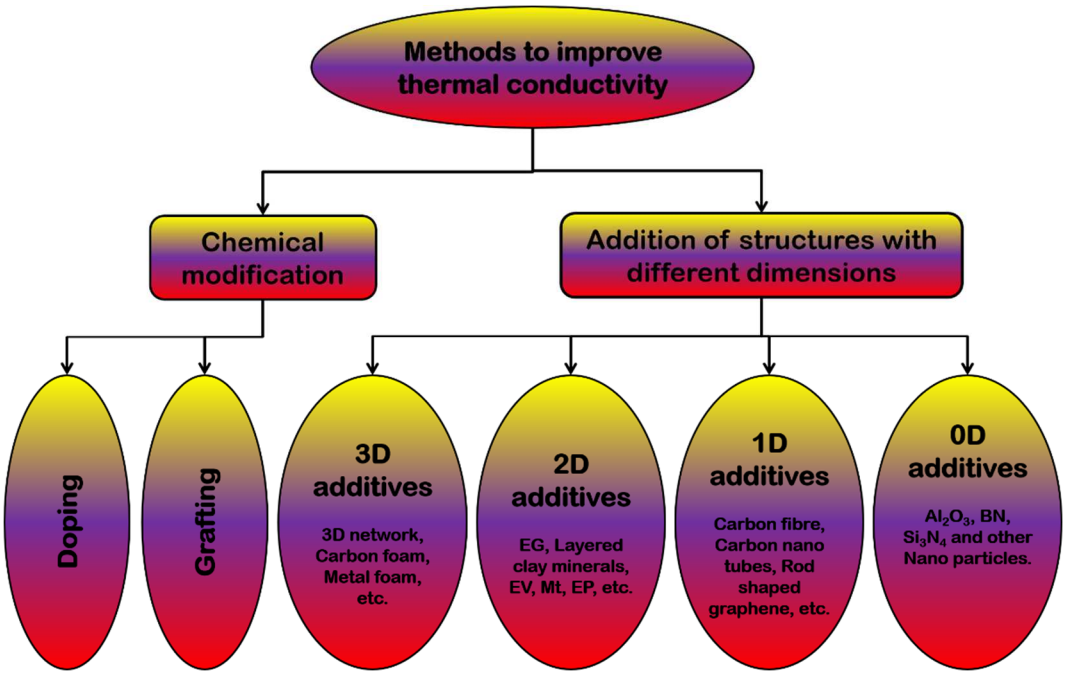

Figure 3 Methods for improving PCM thermal conductivity

3.2.1. ***Chemical modification***

3.2.1.1. Doping

The impact of macroscopic doping on the micromorphology of the composite is primarily expressed in the matrix's pore quantity and size. Doping causes significant changes in the thermal conductive matrix's surface phase composition and structure. It reduces phonon scattering and increases the number of thermal conduction channels. Porous materials obtained with a doped element will improve PCM cyclic stability and thermal conductivity while also improving its microstructure and surface compatibility. Significant research has been done on the doping of the components of the additive substrate. In this regard, Atinafu *et al.* [40] used two synthesis strategies to create mesoporous N-doped carbons/myristic acid-stearic acid (MA-SA) form shape stabilized PCM. Various synthesis techniques and N species present in porous carbons were used to examine the microstructure and thermal energy storage characteristics of the composite PCM. From the obtained results, it was found that the N-doped porous carbons derived from *in situ* (NPC/MA-SA) have a remarkable heat storage capacity of 164.33 kJ/kg with a limit of up to 88 wt% PCM loading. The resulting melting temperature of NPC/MA-SA PCM is 49.45 °C, which is lower than that of the pure PCM, while the thermal increases up to 117.65%, as shown in Figure 4.

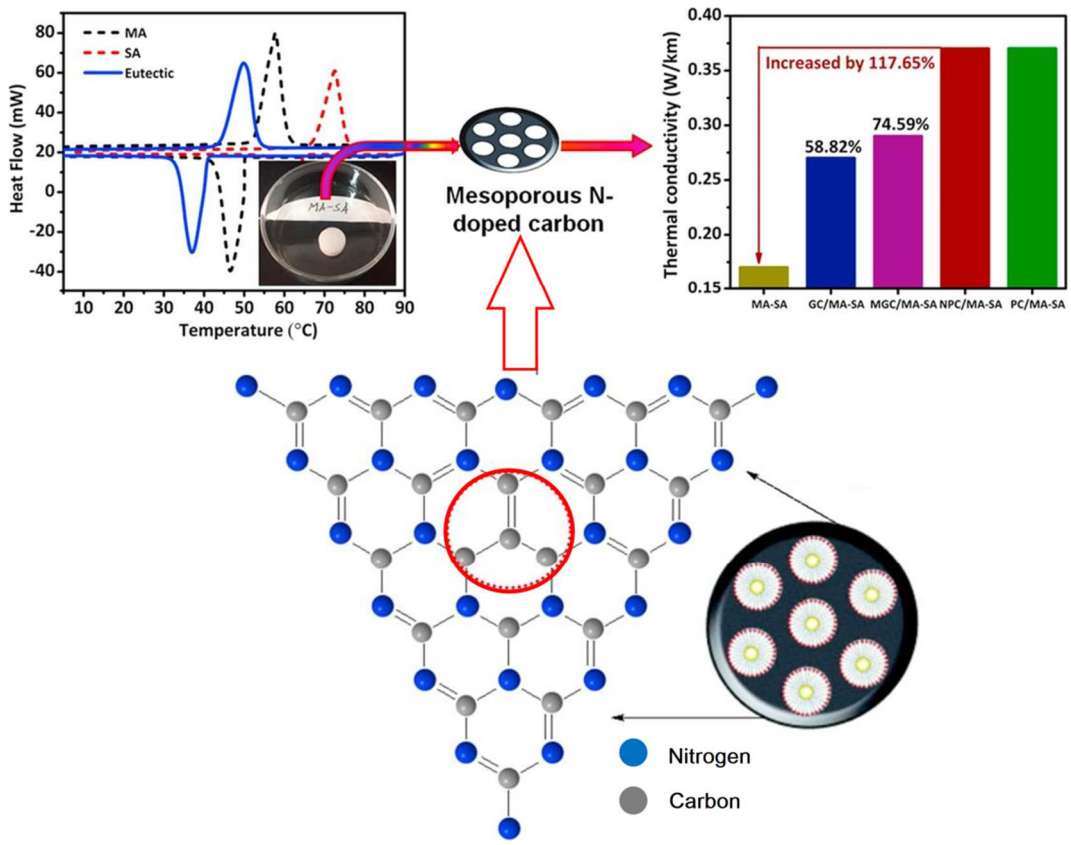

175

176 *Figure 4 Porous carbon matrix/MA-SA composite PCM thermal conductivity and heat flow.*
177 *Reproduced with permission from ref.* [40]*, Copyright (2018) with permission from Elsevier.*

178 Mehrali *et al.* [41] developed a shape-stabilized NDG/palmitic acid (PA) composite PCM
179 with improved thermal conductivity. The TEM and field emission SEM images of the NDG
180 with the PA/NDG composite PCM are presented in Figure 5, revealing the porous structure
181 and randomly stacked nanosheets of NDG, while the adsorption of PA causes a denser
182 structure. NDG was dispersed at different mass fractions (varying from 1% to 5%) in liquid
183 PA using high-power ultrasonication. To quantify the thermal stability and thermophysical
184 properties of the composite, a thermogravimetric analyzer (TGA) and a differential scanning
185 calorimeter (DSC) were used. The thermal conductivity of NDG/PA composite is tested
186 using the laser flash method at 35 ºC, and the results show that with the maximum 5%
187 loading of NDG, the thermal conductivity is increased by 500%. The established composite
188 was submitted to thermal cycle tests up to 1000 cycles, with the results suggesting that the
189 NDG/PA composite has good thermal and chemical stabilities. Chen *et al.* [42] investigated
190 the thermal behavior of organic PCMs with N-doped hierarchical carbon. Their study sheds
191 light on how small molecular organic PCM are confined within a sequestered nanoscale N-
192 doped hierarchical carbon structure. The composite PCM has a superior heat transfer rate as

compared to pure PCM and maximum crystallinity of 90.71%. To produce polyethylene glycol (PEG)-based composite PCM, Atinafu *et al.* [43] synthesized N-doped porous carbon (NPC-Al) applying a one-step NH_2-MIL-53(Al) metal-organic structure. A schematic of the synthesis process is presented in Figure 6. NPC-Al demonstrated homogeneous PEG packing potential (up to 90 wt%), enhanced thermal conductivity (up to 52%), and thermal storage capability (up to 100.3%). Furthermore, the composites demonstrated superior reliability, with 99.5 % retention after 50 heating and cooling cycles without leakage, as well as higher thermal effusivity and specific heat power than pure PEG.

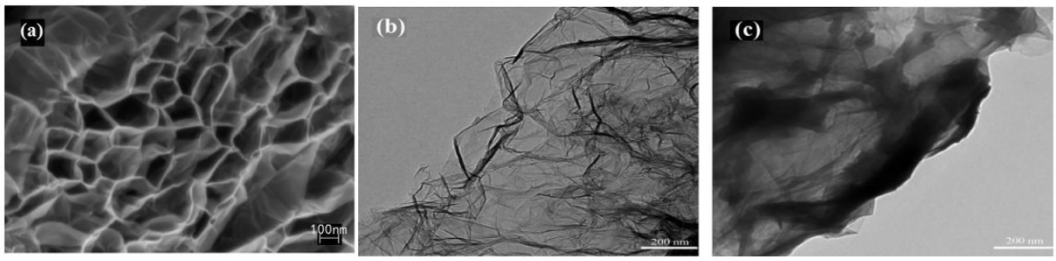

Figure 5 (a) NDG field emission SEM images, (b) NDG TEM images, (c) PA/NDG composite PCM TEM images. Reproduced with permission from ref. [41]*, Copyright (2014) with permission from Elsevier.*

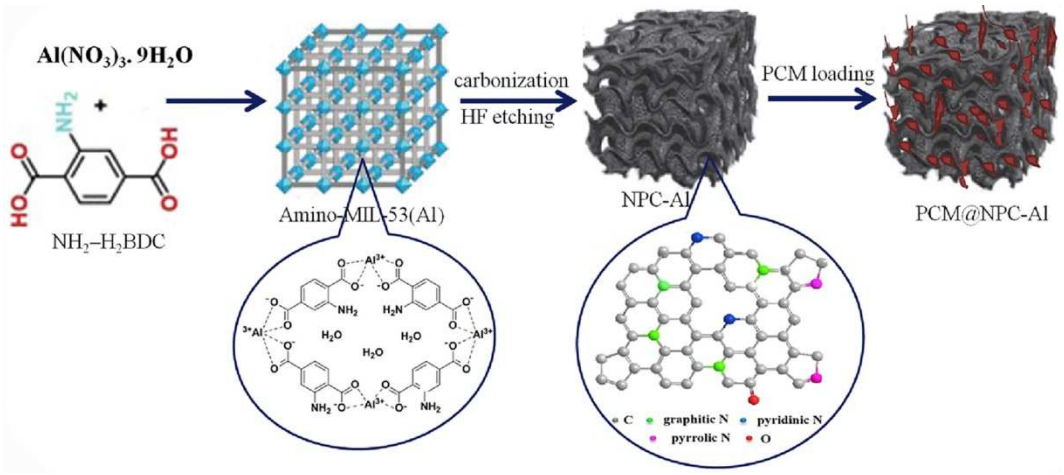

Figure 6 PEG@NPC-Al composite syntheses schematic illustration. Reproduced with permission from ref. [43]*, Copyright (2019) with permission from Elsevier.*

3.2.1.2. Functional groups grafting

Grafting, also referred to as post-synthesis, is a chemical reaction in which organic groups are introduced onto the surface of mesoporous channels. Following grafting, additional

reactions are carried out to generate new active centers. The newly formed active centers have no impact on the matrix material's mesoporous structure in any of the organic functional groups. However, it reduces pore volume by blocking mesoporous channels due to unevenly spaced organic functional groups on the orifice and exterior surface. The following are the characteristics of grafting organic functional groups into composite materials: (i) the pore size of the matrix steadily decreases as the number of organic groups increases, (ii) the mesoporous structure of the matrix material remains unchanged (iii) the form of the organic group may be changed to control the thermal conductivity of composite materials.

The supporting materials are grafted to improve the thermophysical properties of the PCM based on the characteristics discussed above. In this regard, Wang *et al.* [44] used heterogeneous ribbons to develop Cr-MIL-101-NH_2 metal-organic frameworks (MOFs) nanoparticles network structures on the surfaces of carbon nanotubes (CNTs). PCMs were stabilized by MOF nanoparticles, which were absorbed by the capillary force of the porous structure and anchored by the hydrogen bond interaction of amino groups. As seen in Figure 7, the thermal conductivity of the PEG2000/CNT@Cr-MIL-101-NH_2 shape-stabilized PCM composite was 100.9 % higher than that of the PEG2000/Cr-MIL-101-NH_2 PCM composite. The energy storage capability and thermal stability of PEG2000/CNT@Cr-MIL-101-NH_2 over PEG2000/Cr-MIL-101-NH_2 PCM were also increased, according to the findings. Li *et al.* [45] grafted various polyhydric alcohols onto carbon nanotubes (alcohols octanol, tetradecyl alcohol, and stearyl alcohol). CNTs-C8, CNTs-C14, and CNTs-C18 had graft ratio values of 11 %, 32 %, and 38 %, respectively, and CNTs were shortened and evenly distributed after the grafting procedure. The agglomeration of CNTs was minimized [46]. Grafted CNTs/paraffin have significantly higher thermal conductivities than CNTs/paraffin as shown in Figure 8.

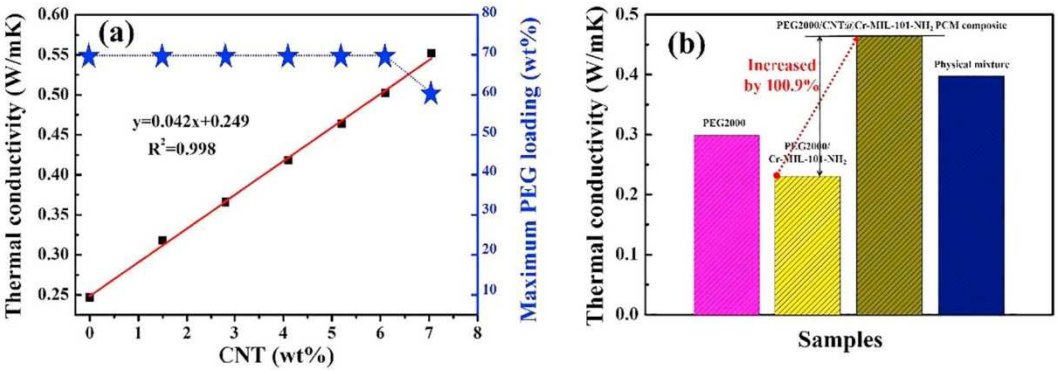

Figure 7 (a) Thermal conductivity of composites containing different CNT mass percentages; (b) A comparison of the prepared composites' thermal conductivity improvement. Reproduced with permission from ref. [44]*, Copyright (2018) with permission from Elsevier.*

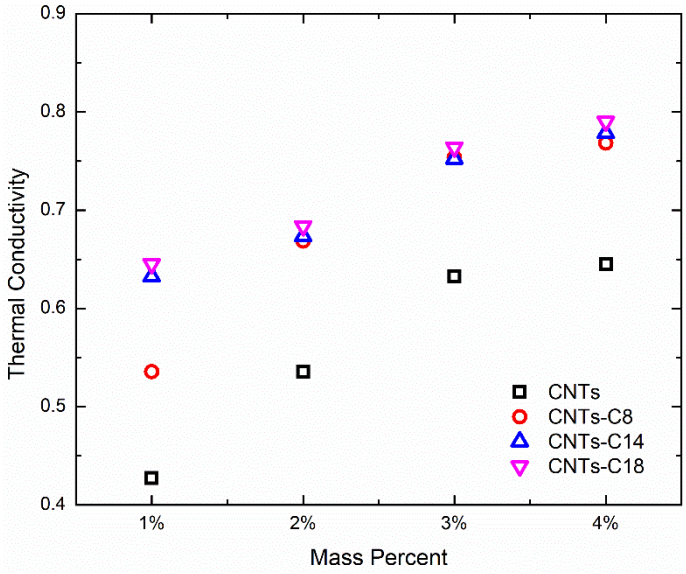

Figure 8 Thermal conductivity of CNTs /paraffin composite PCM. *Reproduced with permission from ref.* [46]*, Copyright (2019) with permission from Elsevier.*

3.2.2. ***Addition of structures with different dimensions***

There are two modes for adding high thermal conductivity materials to PCM. The first approach involves creating a form-stable composite PCM in which the PCM is absorbed in the pores accessible inside the supporting materials, completely preventing leakage as the PCM undergoes a phase change. To minimize phonon scattering and increase thermal conductivity, these PCMs are primarily formed by heat-conducting chains inside the composite, using 3D or 2D organized additives. The resulting materials from this mode are

generally referred to as passive composite PCM. The second approach entails a limited volume of extremely thermally conductive materials being added, to simply improve thermal conductivity. Since liquid PCM leakage cannot be prevented, the formed mixture of PCM and thermally conductive materials is called an initiative composite PCM. Following the addition of the PCM to a 1D or 0D structure, this process creates a heat conduction path.

3.2.2.1. 3D additives for composite PCMs

Many morphological structures exist in 3D structured additives, such as graphite foams (GF), heavily graphitized network carbon and metallic foams, etc. [47]. The additives easily form an integrated pore network and have a conductive pathway for enhancing heat transfer in the PCM due to their composition. The 3D additives are the ideal choice as they increase the thermal conductivity as well as reduce the degree of supercooling [48]. Different studies have been carried out in the recent past to improve the thermal conductivity of PCM using 3D structures. Ji *et al.* [49] added ultra-thin graphite to improve the effective thermal conductivity of a PCM without changing its melting temperature and energy storage capacity. The graphite has high porosity, low density, the high thermal conductivity of up to 200 W/(m K), high thermal stability, corrosion resistance, properties that are compatible with most PCM [50–56]. A highly graphitized 3D carbon network is an attractive matrix with a high thermal conductivity that increases phonon transmission routes. As a result, adding a heavily graphitized 3D carbon network to the PCMs effectively improves the composite PCM thermal conductivity [57–62]. Zhang *et al.* [54] proposed a three-dimensional diamond foam (DF) on Cr-modified Cu foam by template-directed chemical vapor deposition (CVD) as a highly conductive filler for paraffin-based PCM. The thermal conductivity of pure paraffin, diamond particle (DP)/paraffin, copper foam (CF)/paraffin, and diamond foam (DF)/paraffin were 0.25 W/m K, 0.45 W/m K, 2.56 W/m K and 6.70 W/m K, respectively. Even at a very low volume fraction of diamond (1.3 vol%), the thermal conductivity of DF/paraffin was 162% higher than that of CF/paraffin and 2580% higher than that of pure paraffin. Chen *et al.* [57] prepared 3D highly graphitic compact carbon network for providing a superior interconnected path for phonon propagation in the composite PCM. Carbon quantum dots (CQDs) derived from acetone and divinyl benzene (DVB) provide a simple, low-cost, and controlled method for constructing a compactly linked 3D celosia-like highly graphitized thermally conductive network carbon. The novel function of CQDs is first developed for enhanced thermal energy harvesting, thereby expanding their conventional fluorescence and

catalysis field to innovative thermal energy storage. This solution incorporates adequate power capacity as well as the additional thermal conductivity of the PCMs (increased by 236 %). Hu *et al.* [60] enhanced the thermal conductivity of a paraffin phase change material from 0.105 W/(m K) to 9.72 W/(m K) by introducing diamond-carbon nanotube foams, representing one of the highest enhancements ever reported.

The addition of PCM to the metal foam's extremely porous continuous skeleton structure will significantly increase the thermal conductivity of the composite PCM while reducing its heat storage ability to some degree. Copper [63–65], aluminum [66,67], titanium dioxide [68] and nickel [69–71] are the most widely examined metal foams. Abdulmunem *et al.* [72] dispersed nanoparticles within a combination of PCM and copper foam matrix (CFM). The results demonstrate the effect of the bundles of tangled tubes of the multi-walled carbon nanotubes (MWCNTs) additives. With a 0.2% concentration ratio within the PCM/CFM, the effective thermal conductivity was increased from 2.90 W/(m K) to 2.95 W/(m K).

3.2.2.2. 2D additives for composite PCM

Because of its 2D lamellar form which is identical to clay mineral, expanded graphite (EG) is compatible with PCM and avoids leakage. It also features a wide surface area and pore network, which means it has numerous active sites and heat conduction chains, which in turn will enhance the thermal conductivity of the composite PCM [73–75]. The clay network structures result in quicker absorption of PCM into the pore system to form solid PCM. However, because of the small pore openings and the short distance between clay layers, PCM absorption may be reduced in certain situations. The interaction between clay and PCM mainly depends on surface tension, van der Waals forces, capillary force, and hydrogen bond. SiO_2 is used as a supporting material to resist PCM outflow, owing to its three-layer reticulated crystal structure [76–81]. Sepiolite, extended perlite, attapulgite, and expanded vermiculite provide broad unique surface areas [82,83,92–97,84–91]. Jin *et al.* [98] developed a novel sodium acetate trihydrate (SAT)–potassium chloride (KCl)–urea/expanded graphite (EG) composite PCM. EG was infused into the source composite salt to get ready SAT–KCl–urea/EG. The SAT–KCl–urea/EG CPCM, which contains 9 wt% EG, was found to be the best for improving thermal energy storage efficiency without losing phase shift properties. The preparation method of (SAT)–(KCl)–urea/EG CPCM, the enhanced thermal conductivities and the DSC curves at different EG loading are presented in Figure 9. From Figure 9, it can be observed that the thermal conductivity of pure PCM is increased with an

increase in EG loading. Ma *et al.* [99] prepared a series of stearic acid (SA)/benzamide (BA) binary mixtures and EG was impregnated to enhance the thermal conductivity because of its good compatibility. As compared to the eutectic mixture, the thermal conductivity of the composite with 12 wt% EG was improved by 12.30 times. Rathore *et al.* [100] used PCM/expanded vermiculite/expanded graphite shape stabilized composite PCM for building energy applications. The thermal conductivity of the composite PCM was significantly affected by the presence of EG and increased with the increase in mass content of EG. The maximum value of thermal conductivity of 0.311 W/(mK) was obtained with an increment of 114.4% in comparison to the pure PCM.

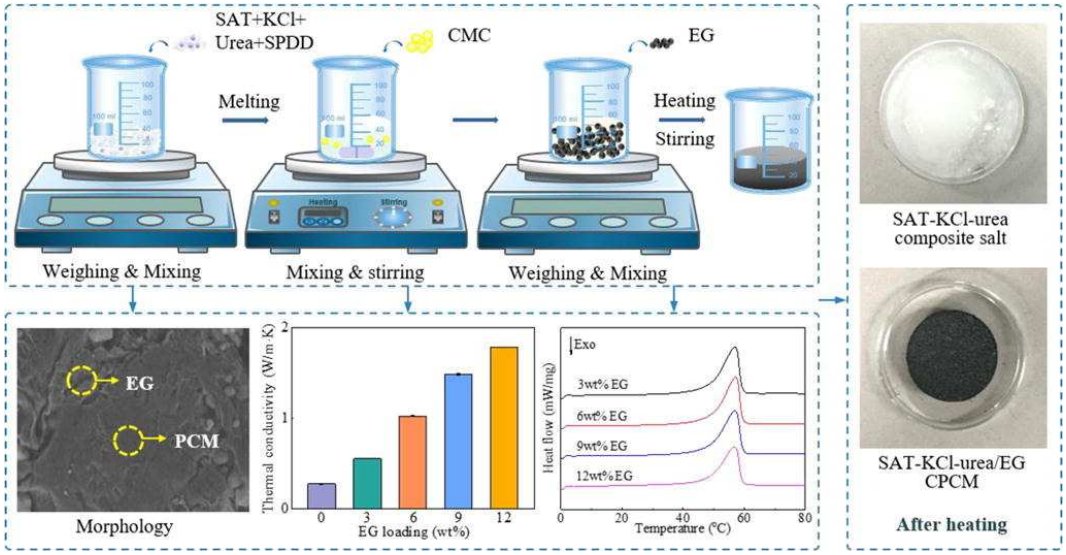

Figure 9 Preparation method of (SAT)–(KCl)–urea/EG CPCM, enhanced thermal conductivities and DSC curves at different EG loading. Reproduced with permission from ref. [98]*, Copyright (2021) with permission from Elsevier.*

3.2.2.3. Initiative composite PCM using 1D additives

Carbon nanotubes (CNTs), carbon fiber (CF), and cylindrical type graphene are only a few of the morphological structures used in 1D form additives. Because of the 1D structure's excellent thermal conductivity, even a limited amount of additives will greatly improve the thermal conductivity. Furthermore, 1D structure additives are lighter than metal additives and minimize supercooling, making them an excellent alternative for a high-performance PCM. High-temperature corrosion resistance, low density, and high thermal conductivity are benefits of CF [101]. It can also absorb almost all organic PCM, making it one of the strongest materials for increasing organic PCM thermal conductivity [102]. To improve

thermal transport and stabilize the form of the PCM, Jiang *et al.* [103] prepared carbon bonded carbon fiber (CBCF) monoliths from graphite fibers. CBCF density ranged from 0.09 to 0.39 g/cm^3, and PCM was filled into the pore of the CBCF. Due to anisotropy in the CBCF material, the thermal conductivity of the composite PCM was directional dependent. According to the findings, the in-plane thermal conductivity of the composite PCM was improved by 18 to 57 times over pure wax, while the out-of-plane thermal conductivity was also increased by 3.7 to 5.5 times. Furthermore, as seen in Figure 10 the thermal conductivity of CPCM increases linearly as the volume fraction of CF increases. In Figure 10, k_c and k_m are composite PCM and pure paraffin wax thermal conductivities respectively, while X_f is the volume fraction of carbon fiber. Qian *et al.* [104] used an impregnation approach to make PEG/SWCNTs nano-composite PCM to increase the thermal conductivity of polyethylene glycol. The measurements revealed that a small amount of SWCNT (4%) significantly increases thermal conductivities of the solid (375%) and liquid states (121 %).

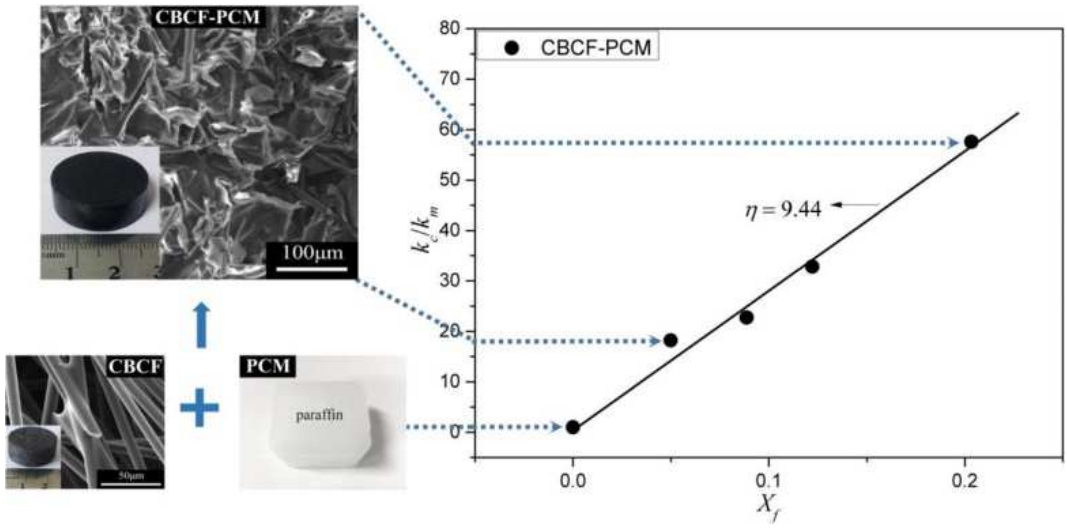

Figure 10 CBCF composite PCM and linearly increase in its thermal conductivity. Reproduced with permission from ref. [103]*, Copyright (2018) with permission from Elsevier.*

Chen *et al.* [105] designed advanced CNT bundles assembled in a flexible hierarchical framework based on PCM composites, for high-performance thermotherapy of allergic rhinitis. Figure 11 illustrates the organic solvent-free self-assembly procedure of a 3D flexible CNT sponge. The bulk product was manufactured by heating a mixture of CNTs, PVDF and NaCl in a specific mold for 3 h in an oven, in which NaCl served as a sacrificial template and PVDF served as a binder. The resulting hierarchical CNT sponge was used as a compatible supporting host and polyethylene glycol (PEG) served as the thermal energy

guest. The constructed flexible CNT sponge-involved composite PCMs assisted by polyvinylidene fluoride (PVDF) yielded high-performance thermotherapy (~33 min of the plateau at ~43.5 °C). Cheng *et al.* [106] developed flexible monolithic PCM based on CNT, chitosan (CS) and poly vinyl alcohol (PVA) using a directional freezing method. The CS/PVA/CNTs (CPC) scaffold was infiltrated with polyethylene glycol (PEG) to prepare PEG@CPC composite PCM. The resulting flexible composite PCM displayed excellent mechanical properties, such as high tensile strength of 2.42 MPa and high bending resistance after 100 cycles. Moreover, it showed very good thermal properties, such as high crystallinity close to 100% and encapsulation ratio of 92.6 wt%.

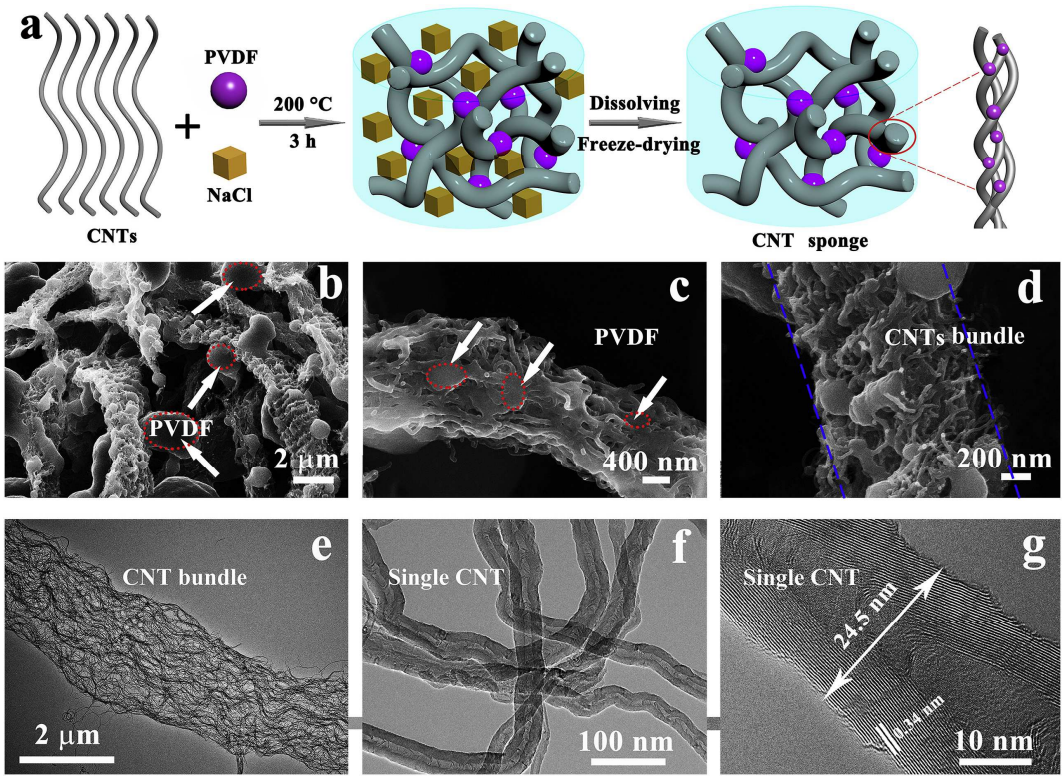

Figure 11 Preparation schematic illustration, (b–d) SEM images, (e–g) TEM images of CNT sponge. Reproduced with permission from ref. [106], Copyright (2020) with permission from Elsevier.

3.2.2.4. Initiative composite PCMs using 0D additives

In the preparation of composite PCM, 0D structure additives have gained a lot of interest. These nanoparticles are ceramic-based and nanoscale-based. Powerful interface interaction, large specific surface region, suitable homogeneity, and good dispersion are all characteristics of 0D standardized additives. Due to their high thermal conductivity, a limited amount of 0D structure additives can greatly increase the thermal conductivity of initiative composite PCMs [107]. Furthermore, inserting nanoparticles in a specific way and proportion improves heat transfer in the composite PCM. Due to the absence of free electrons, heat is

mostly transported by phonons. Several metal oxide additives, such as titanium dioxide (TiO_2), are used in addition to beryllium oxide (BeO) [108–110], aluminum oxide (Al_2O_3) [7], and copper oxide (CuO) [7,111] to give elevated thermal conductivities. Non-oxide additives such as silicon nitride (Si_3N_4) [112], boron nitride (BN) [113–118], silicon carbide (SiC) [96,119], and MOFs [120] have strong interatomic bond energy and crystal structure, which reduces phonon scattering while still providing for high thermal conductivity. Chen *et al.* [121] developed a novel type of MOFs based photoluminescence-functionalized (PL) PCMs for superior thermal energy and fluorescence harvesting using a facile synthetic strategy. The Stearic acid (SA) and carbon quantum dot (CQD) molecules were synchronously incorporated into the Cr-MIL-101-NH_2 framework (Figure 12), in which the MOF framework serves as the support host, CQD as the fluorescent guest, and stearic acid as the thermal energy guest. The fabricated composite PCMs exhibit thermal conductivity of 0.42 W/mK and very good thermal stability, durability, and shape-stabilized ability. Thermal conductivity was enhanced around 1.6 times compared to the pure PCM.

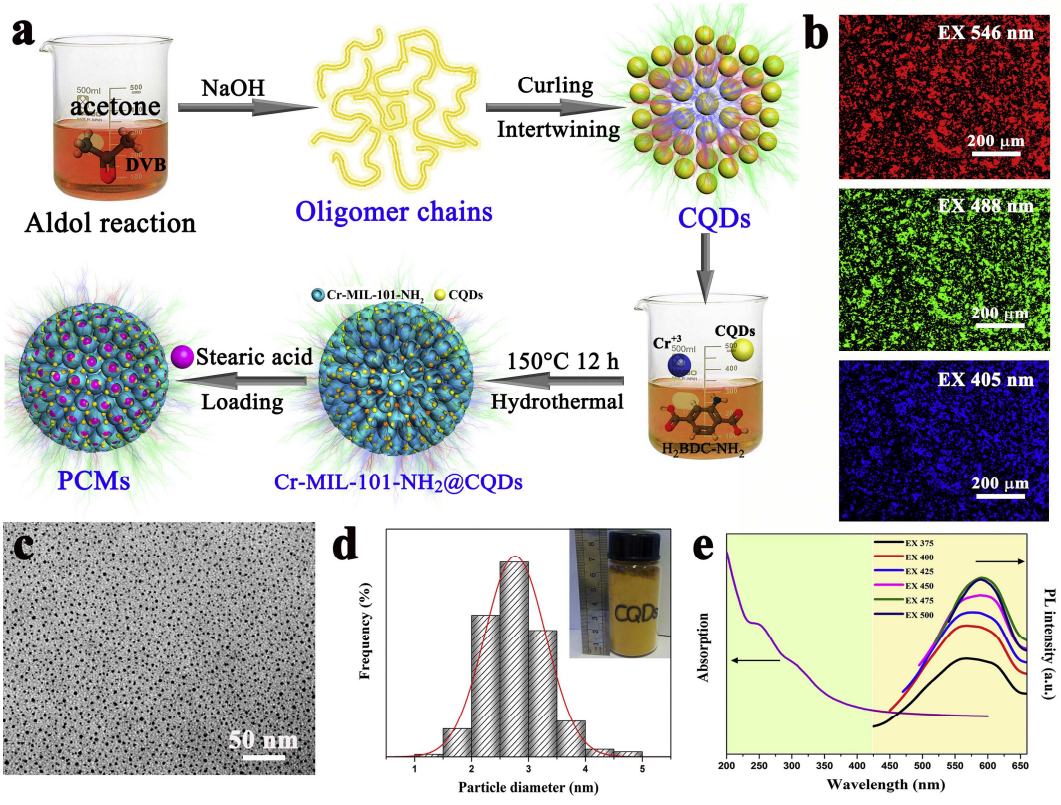

Figure 12 (a) Schematic illustration of photoluminescence-functionalized composite PCM; (b) fluorescent images of pure CQDs at different excitation wavelengths, (c) HRTEM image of pure CQDs, (d) diameter distribution of pure CQDs, the insert is CQDs production, (e) UV–vis absorption spectrum and excitation-independent PL spectra of pure CQDs.

Reproduced with permission from ref. [121], Copyright (2019) with permission from Elsevier.

4. Enhancement of heat storage capacity

Next-generation of PCMs are expected to have increased heat storage capability, which will increase the amount of energy that can be retained during sensible heating and phase transfer cycles. Several studies have been done to enhance the heat storage capacity of base PCM. They have shown that the thermal storage capacity of base PCM can be enhanced by using an appropriate proportion of carbon-based additives like carbon nanotubes (CNTs), carbon nanofibers (CNFs), single and multi-wall carbon nanotubes (SWCNTs and MWCNTs), but also graphene, silica dioxide (SiO_2), alumina (Al_2O_3), titanium dioxide (TiO_2) and the mixture of silica-alumina (SiO_2-$Al2O_3$).

4.1. Enhancement of latent heat of fusion

Although the research has mainly focused on improving the thermal conductivity of paraffin-based PCM, their phase change enthalpies are the main factor that affects the amount of energy that can be retained during the phase transition. To assess the effect of additives on the PCM heat storage potential, the absolute phase change enthalpy (absolute phase change enthalpy = apparent phase change enthalpy/PCM mass fraction) must be measured [122]. The majority of experiments have shown that the additives have little effect or decrease the absolute phase change enthalpy of composite PCM due to the displacement of actual PCM mass (Figure 13) [7,111,123,124]. On the other hand, some recent studies [122,124–127] have found that the thermal energy storage ability of the PCM improves as alkane molecules align around the carbon atoms in carbon-based nanoparticles, owing to the more crystalline structure at the nanoparticle–PCM interface. Figure 13 shows the ratio ε, of absolute phase change enthalpy of nanocomposite paraffin PCMs to the phase change enthalpy of base paraffin PCM [122,128–132], where d is the nanoparticle diameter, and t is the nanoparticle thickness.

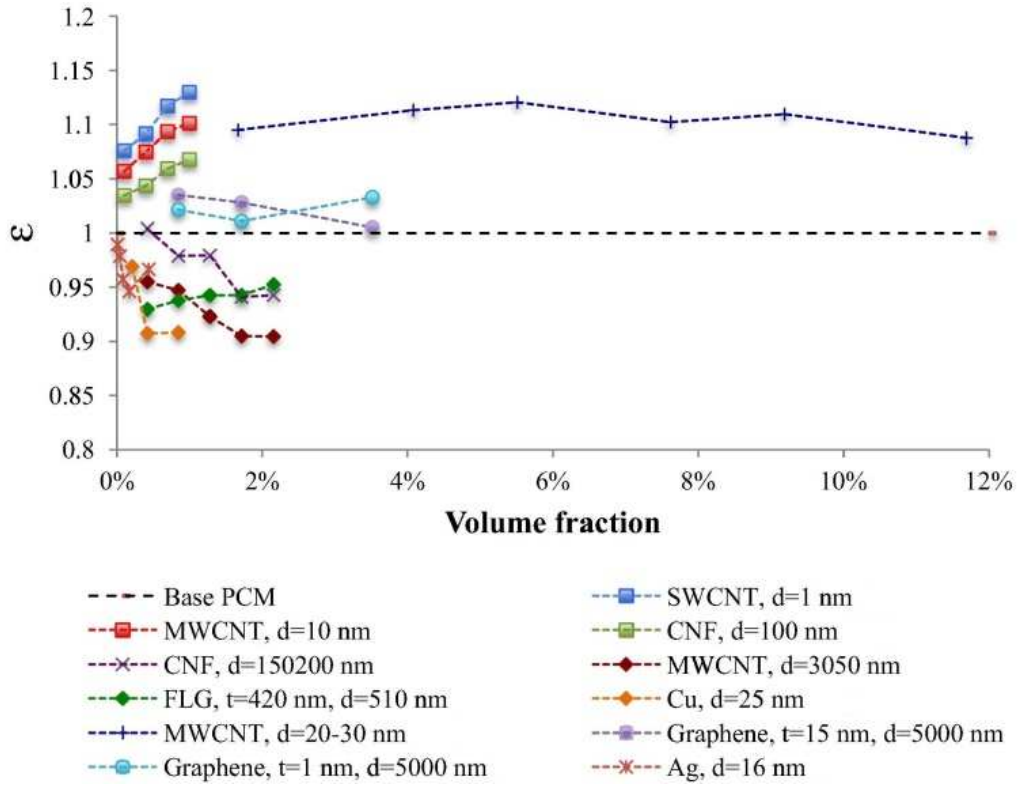

Figure 13 Ratio of absolute phase change enthalpy of nanocomposite paraffin PCMs to the phase change enthalpy of base paraffin PCMs (ε). Reproduced with permission from ref. [124]*, Copyright (2014) with permission from Elsevier*

Experimental work was performed by Warzoha *et al.* [124] to harness thermal energy from the composite PCM using a heat exchanger. The thermal energy extracted during the solidification of MWCNT-paraffin, Al-paraffin, or TiO2 composite PCM at 20% volume loading is about 15-17% lower than that of the base paraffin. The thermal energy extracted by graphene nanoparticle networks (15 nm thickness, 5 μm diameter, 20 v. %) is about 11% higher than for base paraffin (Figure 14). Sun *et al.* [125] used ultra-flyweight, synergistically assembled carbon aerogels and paraffin to create composite PCM. According to the data, the melting and freezing latent heat of the fabricated composite PCM were respectively 7.8% and 28.7% higher than that of paraffin. It was explained by the relationship between paraffin and the hydrophobic surfaces of graphene and CNTs. Li *et al.* [127] looked into the impact of spongy graphene on the latent heat of fusion of a PCM made up of docosane and spongy graphene (G22). The graphene sheets serve as a nucleating agent, increasing the crystallinity of the docosane and thereby increasing the thermal energy storage potential. In a lower graphene concentration of 3 mg/cm^3, the latent heat increased from 256.1 J/g to 262.8 J/g, and the thermal conductivity was more than doubled, as seen in Figure 15. By doping wax

with single-wall carbon nanotubes (SWCNTs), multiwall carbon nanotubes (MWCNTs), and carbon nanofibers, Shaikh *et al.* [130] produced three types of carbon nanoparticles doped PCM. The prepared samples exhibit strong latent heat enhancement as compared to pure shell wax, with a maximum enhancement of 13% for the wax/SWCNT composite equivalent to 1% SWCNT filling. The enhancement of latent heat for the different samples is presented in Figure 16. Lin *et al.* [133] used the solution blending approach to create a new form-stable PCM. The best CPCM sample had a thermal conductivity approximately 4.2 times that of pure PCM and a higher latent heat storage capacity.

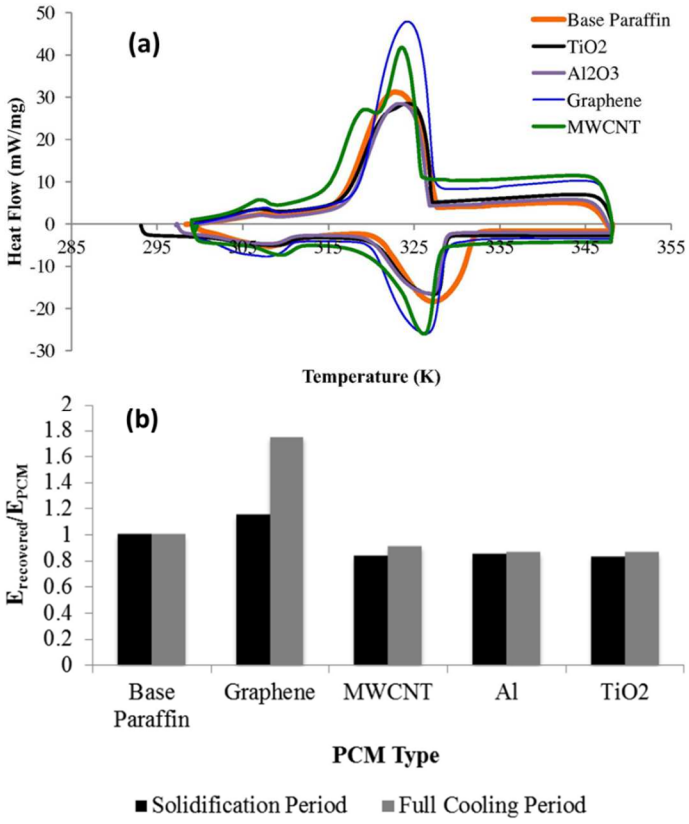

Figure 14(a) DSC heating and cooling curves normalized against PCM mass, (b) the ratio of heat extracted from composite PCM to base paraffin for the solidification time (black bars) and the full cooling cycle (gray bars). Reproduced with permission from ref. [124], *Copyright (2014) with permission from Elsevier*

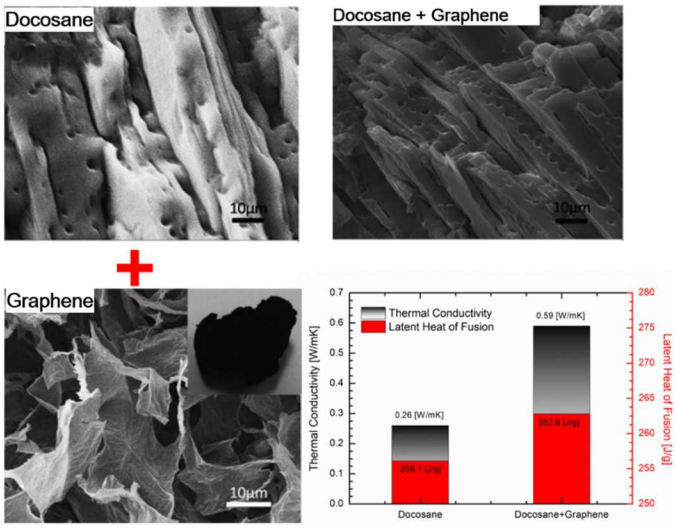

458

459 *Figure 15 Simultaneous enhancement of latent heat and thermal conductivity of*
460 *docosane/graphene composite, Reproduced with permission from ref.* [127], *Copyright*
461 *(2014) with permission from Elsevier*

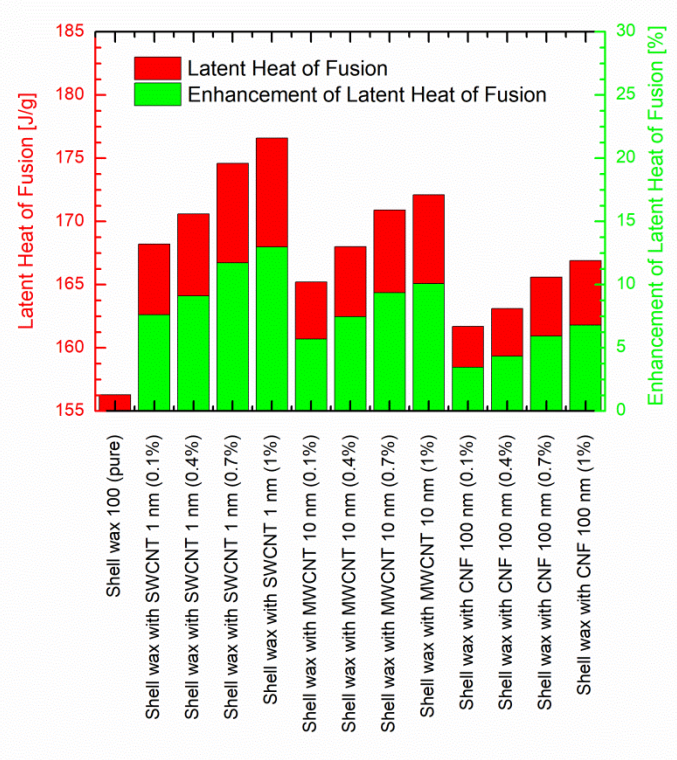

462

463 *Figure 16 DSC values of latent heat of wax and nanoparticle doped composites* [130].

4.2. Enhancement of specific heat capacity

Mehrali *et al.* [41] used nitrogen-doped graphene (NDG) as a supporting medium to create novel form-stable PCM. Based on the additives used, shape stabilization of the PCM addressed leakage problems and changed the thermal conductivity. Figure 17 illustrates the various configurations of PA/NDG composite PCM after drying, with the PA being fully absorbed by NDG particles for the higher NDG mass percentages. The PA had a constant stable form in the mass percentages of 1% and 2%, but this shape was completely modified in other samples due to the absorption of the PA by NDG particles. In temperatures ranging from 35 to 50 °C, the specific heat of pure PA and PA/NDG composite PCM was calculated using the multiple curves method. As seen in Figure 17, the addition of NDG raised the individual temperatures, with the increase becoming more significant for higher NDG loadings.

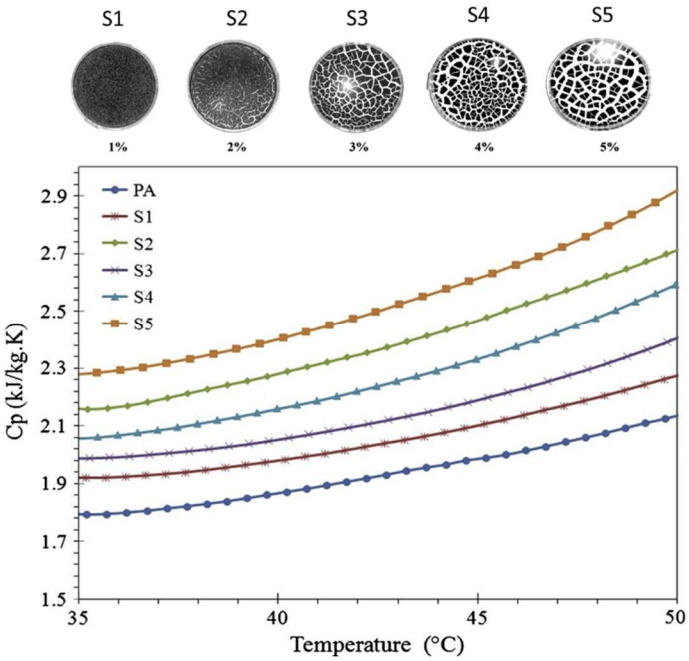

Figure 17 Dried PA/NDG composite PCMs and corresponding specific heat. Reproduced with permission from ref. [41]*, Copyright (2014) with permission from Elsevier*

Shin *et al.* [134] stated that doping silica nanoparticles at 1% mass concentration improves the specific heat capacity of high-temperature nano fluids (alkali metal chloride salt eutectics). The observed 14.5% increase in nanofluid's heat capacity can be explained by three independent competing transport mechanisms: (i) higher specific heat capacity of

nanoparticles than that of bulk silica, (ii) high interfacial thermal resistance between the nanoparticles and fluid, (iii) semi-solid behavior of liquid molecules adhering on the surface of the nanoparticles. Chieruzzi *et al.* [135] developed nano-fluids by direct synthesis of nano-particles and molten salt. A $NaNO_3$-KNO_3 (60:40 ratio) binary salt and silica dioxide (SiO_2), alumina (Al_2O_3), titanium dioxide (TiO_2) and a mix of silica-alumina (SiO_2-Al_2O_3) nanoparticles were used to prepare the nanofluids. According to the results, applying 1.0 % nanoparticles to the base salt increases the specific heat by 15% and 57 % in the solid stage and of 1% and 22% in the liquid state.

The above sections show that a significant amount of research has been devoted to the enhancement of the thermal conductivity, specific heat and latent heat of fusion. However, the efficiency of the energy storage devices also depends on the supercooling and phase segregation behavior of the PCM. The following sections present methods to reduce these drawbacks.

5. Reduction of supercooling

5.1. Mechanism of supercooling

Supercooling refers to a solidification impediment. The material remains in a liquid state even after being cooled below its melting temperature. The presence of supercooling and its amplitude (degree of supercooling) depends on several factors. The most important factors are summarized in Figure 18 and will be detailed hereafter. They are all connected to one major reason for supercooling presence, which is the absence of nucleation sites. Indeed, the initiation of solidification requires a solid particle referred to as a nucleus, which may be too small and even not present at the liquid state. This nucleus is formed and grows by the solidification of the liquid on the solid surface. In this case, the liquid releases its heat to reach minimum energy. The heat release and solid formation depend on the radius r of the nucleus. The released heat is the function of the volume (proportional to r^3) while the solid formation depends on the surface area of the nucleus (proportional to r^2). An energetic barrier is formed for small values of r, which means that the gained surface energy is larger than the heat released by solidification [136]. Liquids enter the supercooled state when energy release from the nucleus necessary to form the solid-liquid interface is not sufficient [137]. In this case, solidification is prevented and the liquid enters into the supercooling state. Solidification initiates when the radius of the nucleus is sufficiently large.

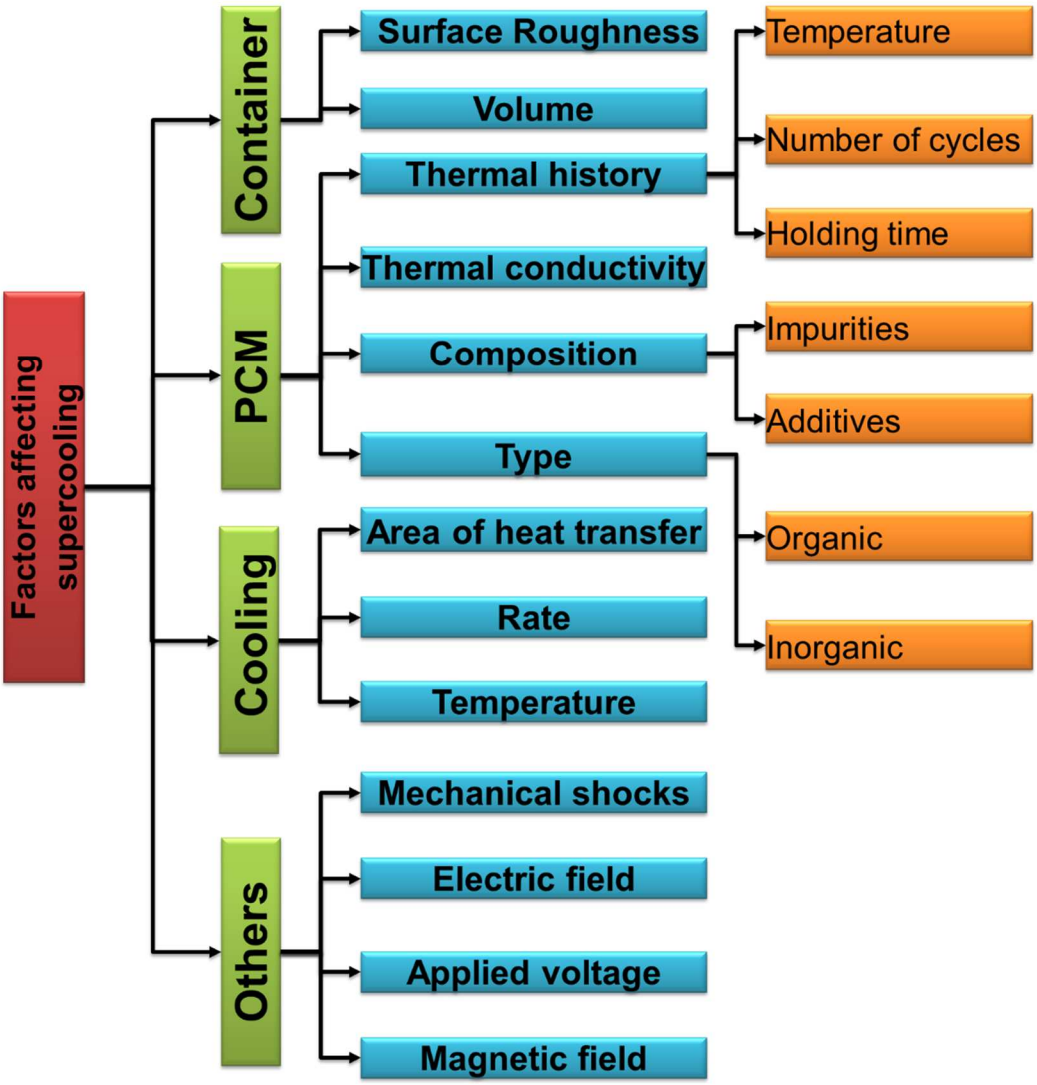

514

515 *Figure 18 Factors affecting the supercooling degree*

516 In PCM based thermal energy storage systems, interruptions in PCM solidification avoid the
517 release of latent heat, causing a problem in the system's engineered solidification-melting
518 period. A PCM is cooled from a temperature T_2 to temperature T_1 or heated from T_1 to T_2
519 exchanges the same quantity of heat. Figure 19 shows the enthalpy change in the cases of the
520 presence or nonappearance of supercooling. In the case of no supercooling, the enthalpy
521 changes according to the black line as temperature drops from T_1 to T_f. As shown in green
522 color, the presence of supercooling prevents solidification and the liquid PCM temperature
523 decreases to the nucleation temperature T_n, where the solidification initiates. Considering the
524 case where a PCM of melting temperature T_m is designed to operate between T_1 to T_2, the
525 PCM will remain in supercooled state upon cooling rather than changing phase. In the case of

supercooling, the released heat will be $(h_1 - h_{2s})$ rather than $(h_1 - h_l) + (h_l - h_s) + (h_s - h_2)$, where $(h_l - h_s)$ is the latent heat. Supercooling is therefore undesirable in most thermal energy storage systems. The difference between the melting point and the temperature at which nucleation begins is the degree of supercooling $(T_m - T_n)$. Supercooling depends on many factors which effects are usually correlated and non-linear. The following sections describe the effects of such factors.

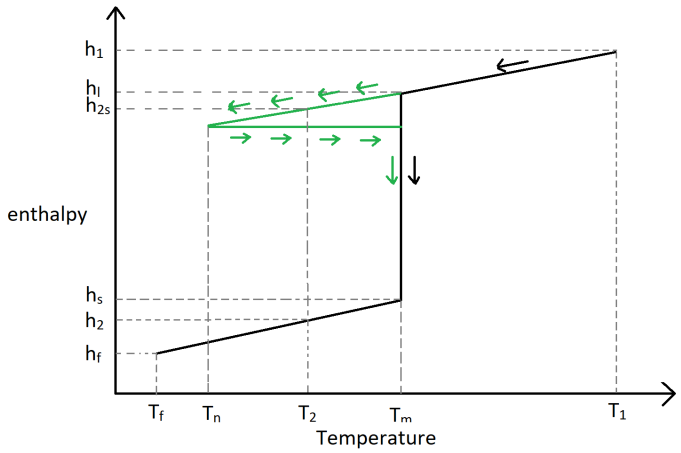

Figure 19 Variation of enthalpy as a function of temperature for the case of no supercooling (in black) and the case of supercooling (in green)

5.2. Methods to reduce supercooling

5.2.1. *Effect of the PCM container volume*

The container in which the PCM is added can affect the degree of supercooling by its surface roughness and volume. As the surface roughness and the volume increase, the degree of supercooling decreases. The rough surface provides a surface of crystallization. As reported by several studies, the solidification of PCM initiates from the scratched (rough) surfaces of the container and any other rough surface introduced in the PCM rather than smooth surfaces [138–142]. The increase in container volume increases the probability of nucleation by increasing the germination sites inside the PCM. Several experiments were held on different PCM, and by changing the volume from cm^3 to mm^3 or from mm^3 to μm^3, the degree of supercooling increased [143–145]. Figure 20 shows the position of nucleation sites of the same PCM encapsulated in different volumes [143]. By increasing the volume from 0.025 cm^3 to 0.4 cm^3 and 16 cm^3, the degree of supercooling decreased from 88 °C to 58 °C and 48 °C respectively. However, the applied techniques to reduce supercooling should not affect the

performance of the PCM based thermal energy storage system. In thermal storage systems, it is better to store PCM in a confined volume. Confining the PCM in many reduced volumes, as it is the case in encapsulation, increases the surface of heat exchange, which in turn enhances the heat transfer rate. Besides, the solidification of the large volume of supercooled liquid leads to the release of a large amount of energy in a short time.

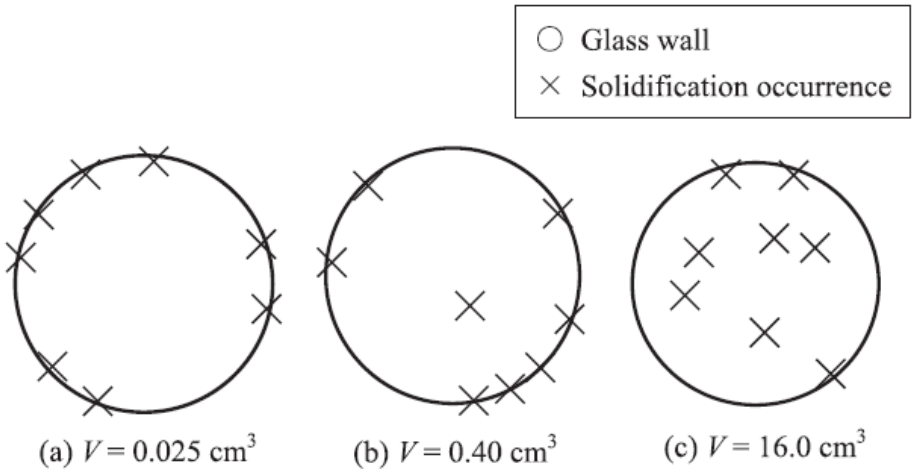

Figure 20 Different solidification site positions for an encapsulated PCM [143]

5.2.2. ***Effect of the cooling rate***

The cooling technique also affects the supercooling of PCM. As mentioned before, increasing the exchange surface area increases the cooling rate. Using a cooling fluid with a temperature higher than the nucleation temperature may lead to the PCM entering supercooling for an undermined time. Increasing the cooling rate for example by further reducing the temperature of the cooling fluid may increase the degree of supercooling but decreases the time spent at the supercooled state because the PCM reaches its nucleation temperature faster. On the other hand, using a low cooling rate (low-temperature difference between cooling fluid and PCM) increases the supercooling time but decreases the supercooling degree.

5.2.3. ***Crystallization inducing methods***

Two methods are generally used to induce crystallization. The first is called manual seeding and is considered very effective [146]. Manual seeding is the addition of seed particles to the supercooled liquid, which triggers crystallization immediately. When crystallization initiates, the temperature increases due to the release of latent heat. As long as the temperature of the

570 liquid is lower than the melting temperature, the crystalline structure continues to spread in
571 the supercooled liquid [147]. The second method is called dynamic stimulation. The
572 supercooled liquid is in an unstable state. Mechanical shocks, ultrasonic vibrations [148],
573 friction [149], agitation [150], magnetic fields [151] etc. can trigger solidification [152,153].

574 5.2.4. ***Change in the PCM formulation: effect of additives***

575 The PCM composition and characteristics also have a direct effect on the degree of
576 supercooling. Nucleation can be homogeneous or heterogeneous. In heterogeneous
577 nucleation, the first nuclei of nucleation initiate from a rough surface, impurities, or additives
578 [154]. On the contrary, homogeneous nucleation occurs suddenly from the liquid with no
579 solid surface aid. Additives serve in decreasing the degree of supercooling to very low values,
580 as found by different experiments [155–158]. However, after a certain percentage, the degree
581 of supercooling increases again, as shown in Figure 21. This is due to the gathering of
582 additives molecules, which reduce their contact surface with PCM molecules. The exact
583 percentage of loading cannot be calculated because of the lack of data on the degree of
584 supercooling for pure materials. The presented values in Figure 21 and Figure 22 are for a
585 given initial value of supercooling. Figure 22(a) shows that for 0 % additive used nucleation
586 cannot occur and the PCM enters in the supercooling state. On the contrary, using 1 %
587 additive almost prevents supercooling. The thermophysical properties of nucleating agents
588 present in additives are very different from that of PCM and modify their chemical
589 composition. The use of these agents should not prevent the PCM from correctly performing
590 its role in the energy storage system [159].

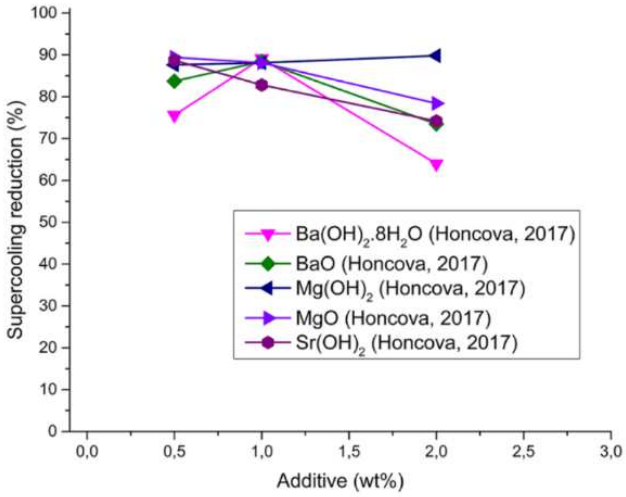

591

592 *Figure 21 Percentage of reduction of supercooling as a function of different additive*
593 *percentages. Reproduced with permission from ref.* [159]*, Copyright (2018) with permission*
594 *from Elsevier*

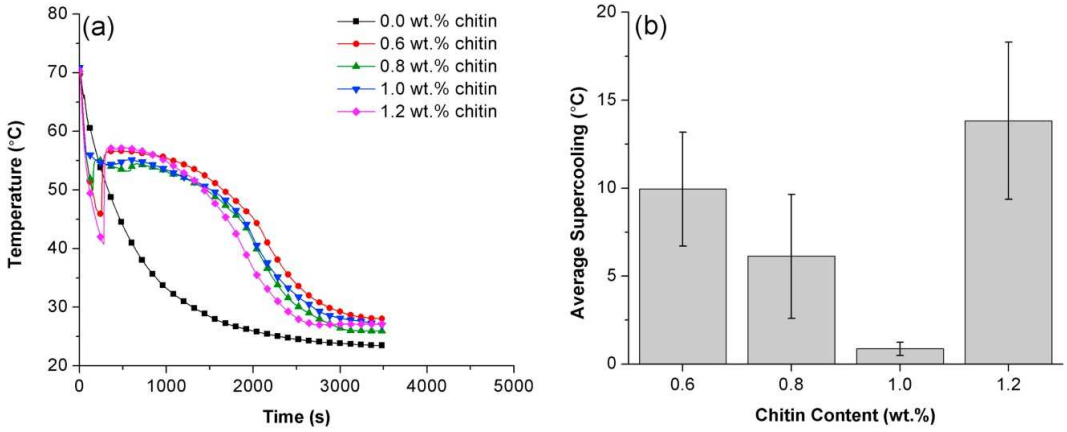

595

596 *Figure 22 Average degree of supercooling for different percentages of additive. Reproduced*
597 *with permission from ref.* [155]*, Copyright (2018) with permission from Elsevier*

598 5.2.5. ***Other factors affecting supercooling***

599 The PCM particle size and the PCM thermal history also affect the degree of supercooling.
600 For PCM initially in powder form, the degree of supercooling increases with the size of the
601 particle. Fashandi and Leung [155] measured the supercooling degree of a series of sodium
602 acetate trihydrate (SAT) PCM, with SAT powder particle size ranging from less than 53 µm
603 to more than 500 µm. As shown in Figure 23a, the supercooling degree increased along, from
604 1 °C to 10 °C. Regarding the thermal history of the PCM, heating a PCM over a certain limit
605 may cause an increase in the degree of supercooling [160]. Figure 23b shows the sudden

increase of the degree of supercooling after heating the PCM over 70 °C [155]. In addition to the heating temperature value, Figure 24 shows that the time held at this temperature also affects the degree of supercooling [161]. Therefore, when integrating PCM in an application, attention should be given to the PCM overheating problem. All other PCM thermophysical characteristics such as latent heat, melting temperature, thermal conductivity, thermal expansion coefficient, etc. are likely in a way or another to change the degree of supercooling.

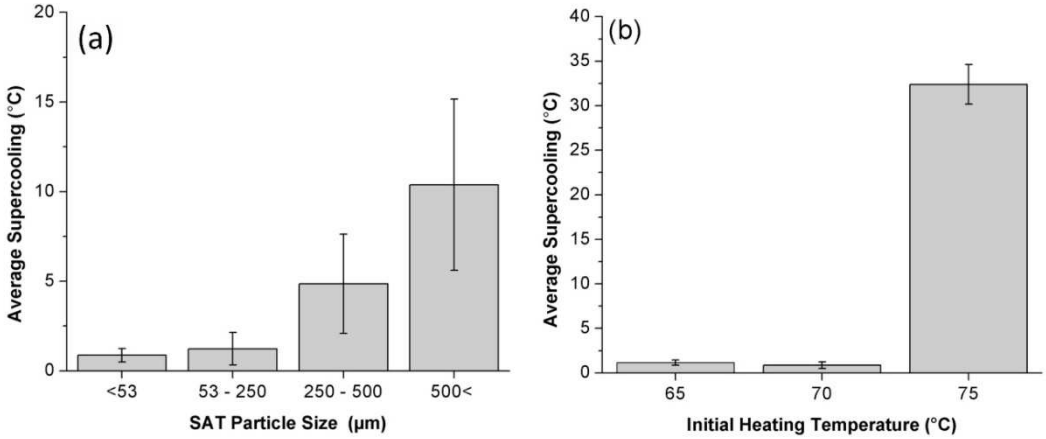

Figure 23 Variation of degree of supercooling as a function of (a) particle size and (b) overheating. Reproduced with permission from ref. [155]*, Copyright (2018) with permission from Elsevier*

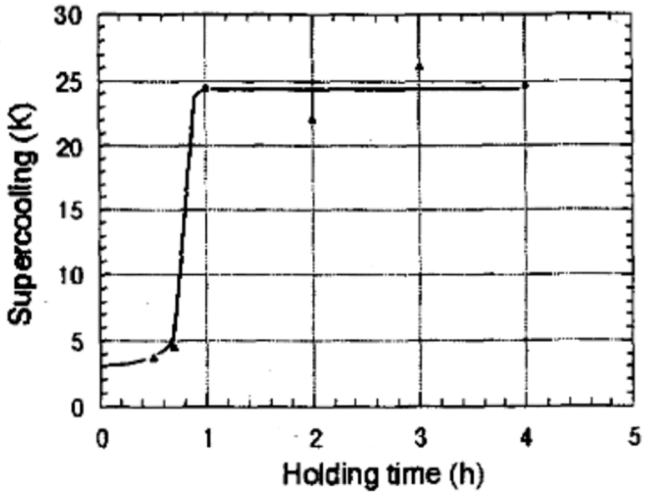

Figure 24 Increase in the degree of supercooling as a function of holding time. Reproduced with permission from ref. [161]*, Copyright (1996) with permission from Elsevier*

6. Reduction of phase segregation

6.1. Mechanism of phase segregation

Heating a pure solid material i.e. a homogeneous material composed of only one type of atom, molecule, or compound, above its melting temperature gives a homogeneous liquid. Solidifying the obtained liquid again yields a solid with the same homogeneous composition, the same phase change temperature and the same phase change enthalpy. In this case, the material is congruently melting. A mixture of two or more materials does not necessarily keep the same behavior under successive heating/cooling processes. Not every multiple component material undergoes phase segregation. Eutectic mixtures solidify simultaneously at the eutectic point and give different solid-phase compositions having the same characteristics as the homogeneous mixture. The eutectic point depends on the concentration of the components in the mixture and on the melting temperature as shown in Figure 25. For that reason, a PCM undergoing supercooling risks having phase segregation. In this case, the eutectic mixture is not a congruent melting mixture.

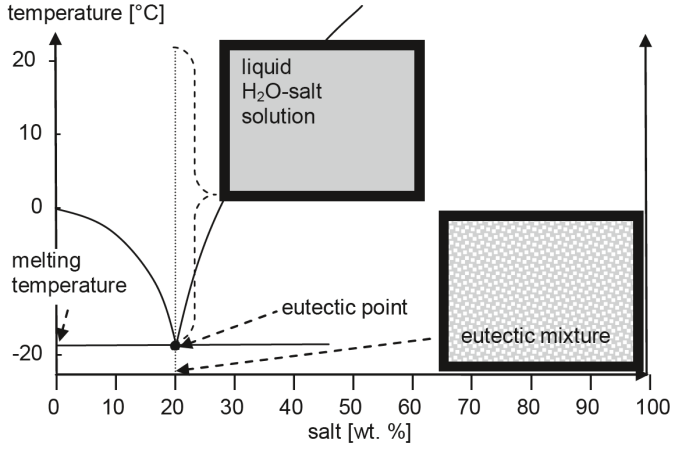

Figure 25 Congruent melting of the eutectic mixture having 20 wt % salt. Reproduced with permission from ref. [136]*, Copyright (2008) with permission from Elsevier*

The behavior of salt hydrates is more complicated than the before mentioned. Using Salt.nH$_2$O with different values of n yields different phase diagrams. For example, the cooling of $CaCl_2 \cdot 6H_2O$ does not directly form solid $CaCl_2 \cdot 6H_2O$. Instead, a solid $CaCl_2 \cdot 6H_2O$ and a liquid $CaCl_2 \cdot 6H_2O$ are formed first, due to the low concentration of salt $CaCl_2 \cdot 6H_2O$ which gives a similar phase change temperature as the solid $CaCl_2 \cdot 6H_2O$, as shown in Figure 26. At this temperature, the solid and liquid phases react to give a single solid solution. The

transformation is known as a *peritectic* transformation which is the transformation of a solid and a liquid to a solid. Above the *peritectic* temperature, a homogenous liquid mixture is obtained. The thermophysical properties of the PCM change during the phase change, which is a disadvantage in regard to phase segregation. If the cooling rate is low, phase segregation of the liquid and solid phases may happen due to density differences. This type of melting is called semi-congruent melting.

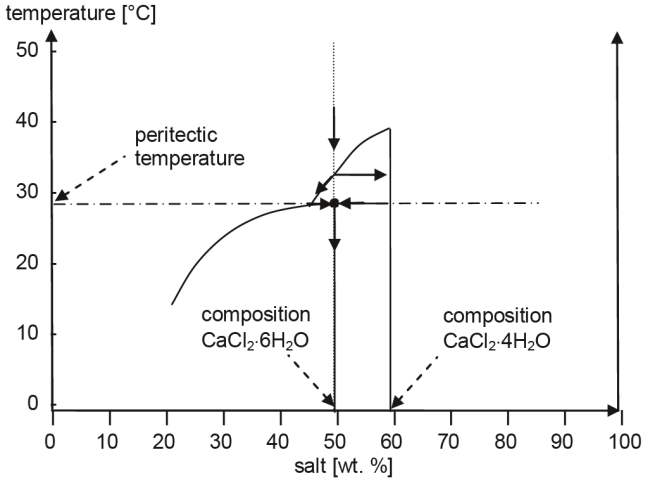

Figure 26 incongruent melting of hydrated calcium chloride. Reproduced with permission from ref. [136], *Copyright (2008) with permission from Elsevier*

6.2. Methods to reduce phase segregation

6.2.1. ***Effect of the mixture homogeneity***

Phase segregation causes a change in thermophysical properties of the PCM that can ruin the system. Several solutions exist to reduce phase segregation. In the preparation of a composite PCM, reducing the density difference among the used compounds may reduce the risk of phase segregation. Indeed, one basic cause for phase segregation is the difference in gravity forces applied within a nonhomogeneous PCM [162,163]. In mixtures of PCM, another cause for phase segregation is the difference in melting temperatures of the used PCM, which leads to incongruent melting [162]. For a given PCM, one solution to insure the homogeneity of a mixture is to use a rotating container [163].

6.2.2. *Effect of thickening agents*

Thickening agents increase the viscosity of the mixture without changing its properties. The experiment held by Ryu *et al.* [164] shows that using 3 to 5 wt% thickening agent on an inorganic PCM was able to remove phase segregation. Zinc nitrate hexahydrate was tested by Kumar *et al.* [165] as a PCM with a high degree of supercooling. By adding 5 wt% zinc oxide nucleating additives, the PCM displayed phase segregation as shown in Figure 27.

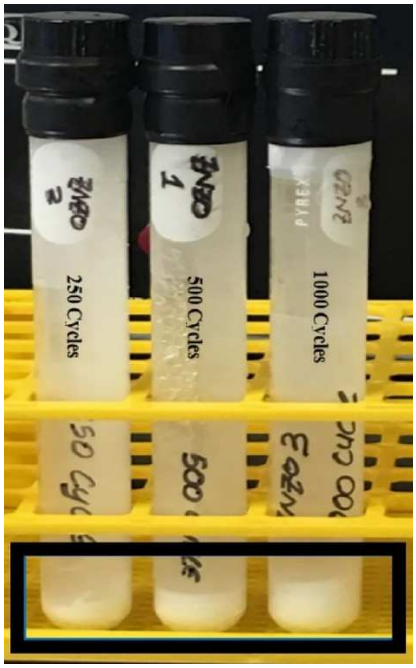

Figure 27 Phase segregation after 250, 500 and 1000 thermal cycles of repeated melting and solidification from left to right respectively. Reproduced with permission from ref. [165], *Copyright (2018) with permission from Elsevier*

In the same experiment [165], using additives (zinc hydroxyl nitrate) allowed to decrease the supercooling degree and the energy loss, but not to eliminate phase segregation after 750 cycles of melting/solidification.

6.2.3. *Effect of the cooling rate*

The cooling rate has a direct effect on the presence of phase segregation. Reducing the cooling rate may reduce phase segregation. Figure 28 shows no phase segregation when cooling a zinc nitrate hexahydrate PCM at 24 °C (cases A and C). However, phase segregation appears when using a cooling fluid of temperature 15 °C, regardless of the

presence of additives (cases B and D). An average value of energy loss due to phase segregation after 750 cycles was estimated at 30kJ/kg.

Other methods to reduce phase segregation include gelling and adding water to the PCM mixture. Table 1 summarizes the most used methods to overcome phase segregation. For each method used, there are several advantages and disadvantages.

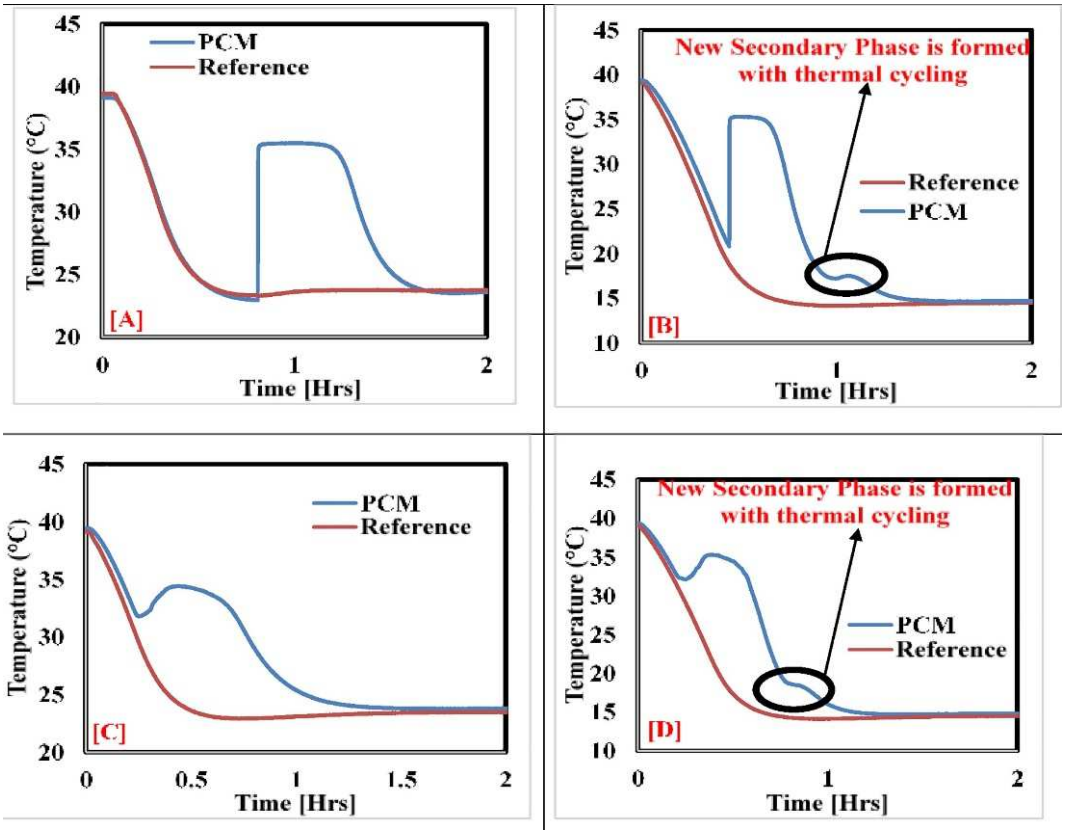

Figure 28 Cooling curves of zinc nitrate hexahydrate after 750 cycles for the cases with additives (C and D) and without additives (A and B) upon cooling at 24 °C (case A and C) and 15 °C (case B and D). Reproduced with permission from ref. [165], *Copyright (2018) with permission from Elsevier*

Table 1 Advantages and disadvantages of different methods to reduce phase segregation

Method	Advantages	Disadvantages
Mixing	Fast process No need to wait for diffusion to obtain a homogeneous mixture	Needed equipment to perform this method

Add water (for salt hydrates)	Faster homogenization by diffusion of $CaCl_2 \cdot 4H_2O$	Decrease storage density Increase phase change range
Diffusion process	Natural process	Efficient for small scale
Gelling	Forms a network that holds the different phases together at the microscopic scale	
Thickening agents	Increase viscosity of the liquid Segregation is prevented until solidification ends	
Adding other materials	Modify phase diagram to obtain congruent melting No restrictions Enhance behavior of PCM	

7. Mathematical modelling of pure and composite PCM

7.1. Modelling of pure PCM

7.1.1. *Stefan problem*

Numerous studies deal with the numerical modelling of a PCM in the melting and solidification processes. They show that convection heat transfer significantly affects the melting process, while the conduction heat transfer is dominant in the solidification of the material. Phase change systems characteristics are difficult to predict due to their non-linear nature and the presence of moving interfaces. This problem is known as the Stephan problem, which assumes the presence of two main domains, the liquid and the solid region, separated by a moving interface [166].

One-dimensional mathematical models can be formulated using assumptions such as a constant latent heat, fixed melting temperature, without mushy zone and without super-cooling phenomena [167].

Heat transfer problem in the solid part is expressed through the head diffusion equation:

$$\rho C_S \frac{\partial T_S}{\partial t} = \nabla.(\lambda_S \nabla T_S) + \dot{q}_{v,s} \quad \forall \, x \in D_S \tag{1}$$

which also applies in the liquid part:

$$\rho C_L \frac{\partial T_L}{\partial t} = \nabla.(\lambda_L \nabla T_L) + \dot{q}_{v,L} \quad \forall \, x \in D_L \tag{2}$$

Heat balance at the sharp front interface, namely the Stefan condition, reads:

$$\lambda_S \nabla T_S.\,n - \lambda_L \nabla T_L.\,n = \rho L \frac{d\overline{X}}{dt}.\,n \quad \forall \, \overline{X} \in D_{interface} \tag{3}$$

where ρ is the density, T_S and T_L are the temperatures of the PCM in solid and liquid phase respectively and $\lambda_S = \lambda_S(T_S, x)$ and $\lambda_L = \lambda_L\,(T_L, x)$ are the thermal conductivities of the solid and liquid phase respectively. $C_S = C_S(T_S, x)$ and $C_L = C_L(T_L, x)$ are the heat capacities of the solid and liquid phase respectively and $\dot{q}_{v,s}$ and $\dot{q}_{v,L}$ are source terms. Besides, t stands for the time, n for the unit normal vector on the interface, $\frac{d\overline{X}}{dt}$ for its velocity and L for the latent heat.

Research has overcome the Stefan problem by assuming a simplified 1D model to determine the temperature range in the liquid, solid and interface zones [168–170]. Further research [171] studied the three distinct regions in a PCM (solid, liquid and mushy zone) by using computational fluid dynamics. Sciacovelli *et al.* [172] showed the importance of taking into account both the conduction and convection heat transfer modes since they can both affect the phase change process of the material.

In general, two separate methods, the fixed grid method and the deforming grid method, can be used to numerically implement the set of partial differential equations governing the phase change. The first one leads to straightforward mathematical calculations and determines the melting front by the temperature or the enthalpy distribution. In this approach, fixed grid nodes can help to track the liquid-solid interface. These models were first described in [173–175] and are now very popular among researchers, due to their easy and straightforward implementation. The second method yields a more complex implementation since the grid must deform to track the solid-liquid interface. Besides, it requires the existence of a liquid layer at the start of the simulation. Two main approaches are used within the deforming grid method, namely the *h*-approach and the *r*-approach. The h-approach starts with a uniform

grid and adds or removes mesh points to improve accuracy with each iteration, necessitating the use of data structures [176]. The r-approach also begins with a uniform grid, but it shifts the mesh at each iteration while maintaining the number and topology of the mesh fixed [177,178],[179,180]. In the context of the fixed grid method, many models can be found in the literature, including the enthalpy-porosity formulation, the temperature-transforming model (TTM), the analogous thermal capacity method, the Lattice Boltzmann Method (LBM), which are described in the following sections. Figure 29 summarizes the most common methods used to solve the Stephan problem.

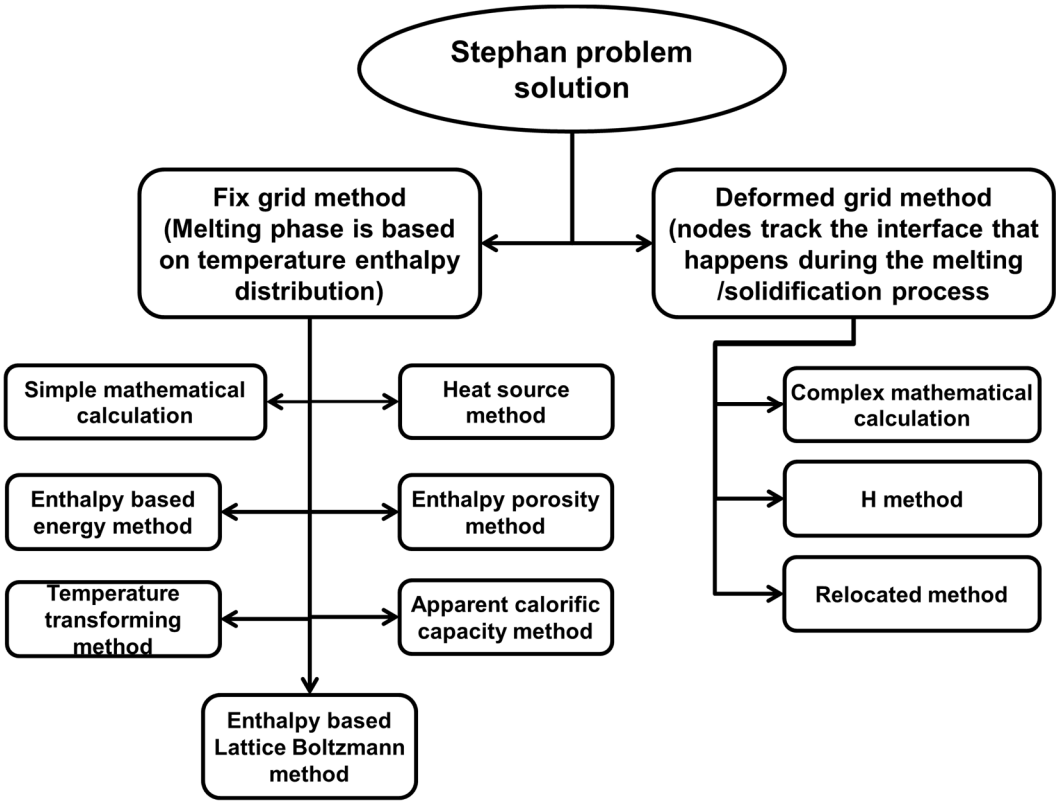

Figure 29 Diagram resuming the different methods used to model the phase change process

7.1.2. ***Enthalpy-based energy method***

Eyres *et al.* [175] proposed the enthalpy-based energy method to solve diffusion phase change problems. The equations of this method are based on the basic equations of heat conduction. The enthalpy *f(T)* of a PCM can be calculated by applying equations (4) and (5) respectively for an isothermal and a non-isothermal phase change, assuming a constant heat capacity and a linear expression for *f(T)* in each phase:

$$f\ (T) = \begin{cases} \rho C_s T & if\ T \le T_m \\ \rho\left(C_s T_m + L + C_L(T - T_m)\right) & if\ T > T_m \end{cases} \quad (4)$$

$$f\ (T) = \begin{cases} \rho C_S T & if\ T \le T_S \\ \rho\left(C_S T_S + L\frac{T - T_S}{T_L - T_S}\right) & if\ T_S < T \le T_L \\ \rho\left(C_S T_S + L + C_L(T - T_L)\right) & if\ T > T_L \end{cases} \quad (5)$$

Voller *et al.* [181–183] used this method while solving a 1D problem with an isothermal phase change. Costa *et al.* [184] also validated the method in presence of conduction and convection by using the finite difference method. Stephan's problem was also solved by the enthalpy method by using Neumann-type boundary conditions and the finite difference method [185]. Vyshak and Jilani [186] modified this method by decoupling the temperature from the liquid fraction.

7.1.3. ***Temperature transforming model (TTM)***

Cao and Faghri [187] suggested the TTM include the natural convection effect while modeling the phase-change problem. Except for the energy equations, which are different from the enthalpy-based energy equations, the equations are similar to that the fluid flow models. The governing equations are as follows:

Continuity equation:

$$\frac{\partial(\rho u)}{\partial x} + \frac{\partial(\rho v)}{\partial y} = 0 \quad (6)$$

Momentum equation:

$$\frac{\partial(\rho u)}{\partial t} + \frac{\partial(\rho u u)}{\partial x} + \frac{\partial(\rho v u)}{\partial y} = -\frac{\partial p}{\partial x} + \frac{\partial}{\partial x}\left(\mu\frac{\partial u}{\partial x}\right) + \frac{\partial}{\partial y}\left(\mu\frac{\partial u}{\partial y}\right) \quad (7)$$

$$\frac{\partial(\rho v)}{\partial t} + \frac{\partial(\rho u v)}{\partial x} + \frac{\partial(\rho v v)}{\partial y} = -\frac{\partial p}{\partial y} + \frac{\partial}{\partial x}\left(\mu\frac{\partial v}{\partial x}\right) + \frac{\partial}{\partial y}\left(\mu\frac{\partial v}{\partial y}\right) + \rho g[\beta(T^*) - 1] \quad (8)$$

Energy equation:

$$\partial\frac{\rho C\mathrm{T}^*}{\partial t} + \partial\frac{\rho u C\mathrm{T}^*}{\partial x} + \partial\frac{\rho v C\mathrm{T}^*}{\partial y} = \frac{\partial}{\partial x}\left(\frac{\lambda\backslash partial\mathrm{T}^*}{\partial x}\right) + \frac{\partial}{\partial y}\left(\frac{\lambda\backslash partial\mathrm{T}^*}{\partial y}\right) - \partial\frac{\rho Cs}{\partial t} - \partial\frac{\rho u Cs}{\partial x} - \partial\frac{\rho v Cs}{\partial y} \quad (9)$$

$$\begin{cases} c = C_S & if\ \mathrm{T}^* < -\Delta T \\ c = \frac{(C_S + C_L)}{2} + \frac{h}{2\Delta T} & if -\Delta T \le \mathrm{T}^* \le \Delta T \\ c = C_L & if\ \mathrm{T}^* > \Delta T \end{cases} \quad (10)$$

$$\begin{cases} s = \Delta T & if\ \mathrm{T}^* < -\Delta T \\ s = \Delta T & if -\Delta T \le \mathrm{T}^* \le \Delta T \\ s = \left(\frac{C_S}{C_L}\right) \Delta T + \frac{h}{C_L} & if\ \mathrm{T}^* > \Delta T \end{cases} \quad (11)$$

$$\begin{cases} \lambda = \lambda_S & if\ \mathrm{T}^* < -\Delta T \\ \lambda = \lambda_S + \frac{(\lambda_L - \lambda_S)(\mathrm{T}^* + \Delta T)}{2\Delta T} & if -\Delta T \le \mathrm{T}^* \le \Delta T \\ \lambda = \lambda_L & if\ \mathrm{T}^* > \Delta T \end{cases} \quad (12)$$

with u the velocity in x-direction, v the velocity in the y-direction, T^* the scaled temperature defined as $T^* = T - Tm$, β the thermal expansion coefficient, h is the latent heat, ΔT the half range of temperatures in the mushy zone, and C the specific heat. $T^* < -\Delta T$ gives the temperature of the solid zone, $-\Delta T \le T^* \le \Delta T$ the temperature of the mushy zone, and $T^* > \Delta T$ the temperature of the liquid zone.

This method was used by Wang et al [188] to study the melting process in a 2D square geometry in presence of natural convection. Different researchers [188–190] proposed a velocity correction in the solid medium and used a consistent update technique (CUT) algorithm to solve the velocity-pressure coupling. Corrections were proposed to obtain zero velocity in the solid zone and were referred to as switch-off, ramped switch-off, variable viscosity and Darcy source term techniques.

7.1.4. ***Enthalpy-Porosity method***

The enthalpy-porosity method is one of the most widely used approaches for modeling phase-change problems in presence of natural convection [191]. In this method, the liquid fraction is determined at each iteration. It is 1 in the liquid phase and 0 in the solid phase. Liquid Fractions between 0 and 1 are obtained for the mushy zone in quasi-porous mediums [192]. The momentum equations are the same as in the TTM method but the method adds two porosity functions named Darcy terms A_u and A_v that allow reducing the velocities gradually in the solid phase. The energy and the total enthalpy in this method can be expressed by:

Energy equation:

$$\partial\frac{\rho h}{\partial t}+\partial\frac{\rho uh}{\partial x}+\partial\frac{\rho vh}{\partial y}=\frac{\partial}{\partial x}\left(\alpha\frac{\partial h}{\partial x}\right)+\frac{\partial}{\partial y}\left(\alpha\frac{\partial h}{\partial y}\right)-\partial\frac{\rho\Delta H}{\partial t}\ -\ \ \partial\frac{\rho\Delta H}{\partial x}\ -\ \partial\frac{\rho\Delta H}{\partial y} \quad (13)$$

Total enthalpy:

$$H=h\ +f_L.L \quad (14)$$

where h is the sensible enthalpy, f_L is the liquid fraction and L is the latent heat. The change in density value between the solid and liquid phases is calculated by $\rho=\rho_L f_L+\ (1-f_L)\rho_s$, the thermal conductivity by $\lambda=\lambda_L f_L+(1-f_L)\lambda_S$ and the specific heat by $C=C_L f_L+(1-f_L)C_s$.

7.1.5. ***Enthalpy based -Lattice Boltzmann Method***

Lattice Boltzmann method (LBM) was used to analyze the melting process in porous materials that includes natural convection [193–195]. This method offers numerical stability and high accuracy. It can be set up for complex geometries. The LBM is advantageous since it has a high parallel implementation of the algorithm [196]. The energy-based method is applied to model the phase change problem and then the LBM comes to solve the fluid flow equations. The Boltzmann equation reads:

$$\frac{\partial f}{\partial t}+\frac{d\overline{X}}{dt}.\nabla f=\Omega \quad (15)$$

where f is the one-particle distribution function at time t, and Ω is an integrodifferential component that relates to the collision operation. Collisions are responsible for making the distribution function close to the equilibrium distribution. Gross *et al.* [197] introduced a new model that approaches closer to the equilibrium by adding a constant relaxation time τ_f that concerns the viscosity of the fluid. The equation (15) becomes:

$$\frac{\partial f}{\partial t}+e.\nabla f=\frac{1}{\tau_f}(f^{eq}-f) \quad (16)$$

where f^{eq} is an equilibrium distribution function and *e* the velocity at time *t*. The LBM offers solutions for complex problems by using the morphological development of complex boundaries [198]. In this method, both micro and mesoscale physics are incorporated and the explicit calculation, leading to time-efficient simulations. Besides, large-scale computational problems can be addressed by LBM.

The mathematical description of microscopic and mesoscopic phenomena in PCM can face many challenges as described by Chatterje [198]. The accuracy of the performance of LBM simulations is influenced by the determination of the thermophysical properties of the substance and the uncertainty of the boundary between the two phases.

7.2. Modelling of enhanced PCM

7.2.1. *PCM with metallic nanoparticles foams and structures*

As shown in Sections 3 and 4, the metallic additives in a PCM are likely to enhance its thermal conductivity and its melting enthalpy. These two parameters can affect the performance of the material since the heat storage rate and the heat storage density are determined respectively by the thermal conductivity and the melting enthalpy. Metallic nanoparticles, foams and structures are known for their strong ability to blend into the host material. In order to study the PCM melting enthalpy reduction produced by the use of nanoparticles, Zhao *et al.* [199] adopted the molecular dynamics method to reveal and analyze the behavior of the material. The first model contained one CuO nanoparticle with different dimensions and 200 n-octadecane paraffin molecules. The interaction between molecules was studied based on CHARMM (Chemistry at HARvard Macromolecular Mechanics) equations [200]. The NPT, or isothermal-isobaric ensemble, and the NVE, or micro-canonical ensemble, were used in the simulation. The results showed that the melting enthalpy quickly decreased with the increase of nanoparticle mass fractions. For 19.72 wt% nanoparticles, the melting enthalpy of the nanoparticle/paraffin decreased by around 51.5 %. As the mass fraction increased, the influence of molecule interactions decreased. It was found that the melting enthalpy reduction was caused by the presence of a dense phase surrounding the nanoparticle [199].

Sciacovelli *et al.* [172] also investigated the thermal properties enhancement of a PCM by nanoparticles (copper powder) dispersion. The simulations were done using a CFD model using the enthalpy method. Results presented an increase in the thermal performance of the material. The melting time was decreased by 15% when the heat flux increased by 16% with 4% of particle volume fraction. Besides, the nanoparticles affected the phase change process since it was noticed a melting time reduction when the mass flow rate was increased. Similar simulations were carried out by Sheikholeslami *et al.* [201] to model the melting process with nanoparticles using the enthalpy-porosity method implemented in ANSYS FLUENT

software. The properties of the nanoparticle-enhanced PCM (NEPCM) were calculated by using the single-phase model equations. This study confirmed the influence of nanoparticles on the thermal behavior of the material. The NEPCM melted faster than the PCM. It was clear that the nanoparticles increased the heat transfer and the melting time was shorter than in the PCM.

Di Giorgio *et al.* [202] developed a mathematical model to study the phase change process and characterize a metallic foam/PCM composite. The model was created using both the volume of fluid (VOF) approach and the volume average technique (VAT). The liquid PCM was assumed incompressible, Newtonian, and depending on the Boussinesq approximation. Besides, the density of the paraffin was supposed constant during melting. The volume-averaged equations used the continuity equation, the averaged momentum balance equation, and the energy balance equation. The heat transfer coefficient for the model without convection was calculated by:

$$U = \frac{1}{t_f}\int_0^{t_f} \frac{\dot{q}_{p-f}(t)}{T_f(t)-T_{PCM}(t)}\,dt \tag{17}$$

where $\dot{q}_{p-f}(t)$ is the heat flux between the PCM and the metal additive, $T_f(t)$ and $T_{PCM}(t)$ are the temperatures of the foam and the PCM, respectively. For the same model but with convection, the heat transfer coefficient was found by calculating the velocity in the first iteration and using it as an input condition for the simulation with atmospheric pressure at the outlet. Moreover, the researcher considered a uniform temperature for the energy equations. This system was solved by using COMSOL software. The numerical model findings were compared to the experimental results and showed good agreement. Atkin and Farid [203] estimated the thermal performance and the viability of using an external finned heat sink through a MATLAB model. One of the studied cases was that of a photovoltaic cell combined with about 30 mm thick PCM infused graphite and aluminum heat sink as shown in Figure 30. The finned heat sink increased the effective area from 0.052 to 0.238 m^2, resulting in a surface ratio of 4.58.

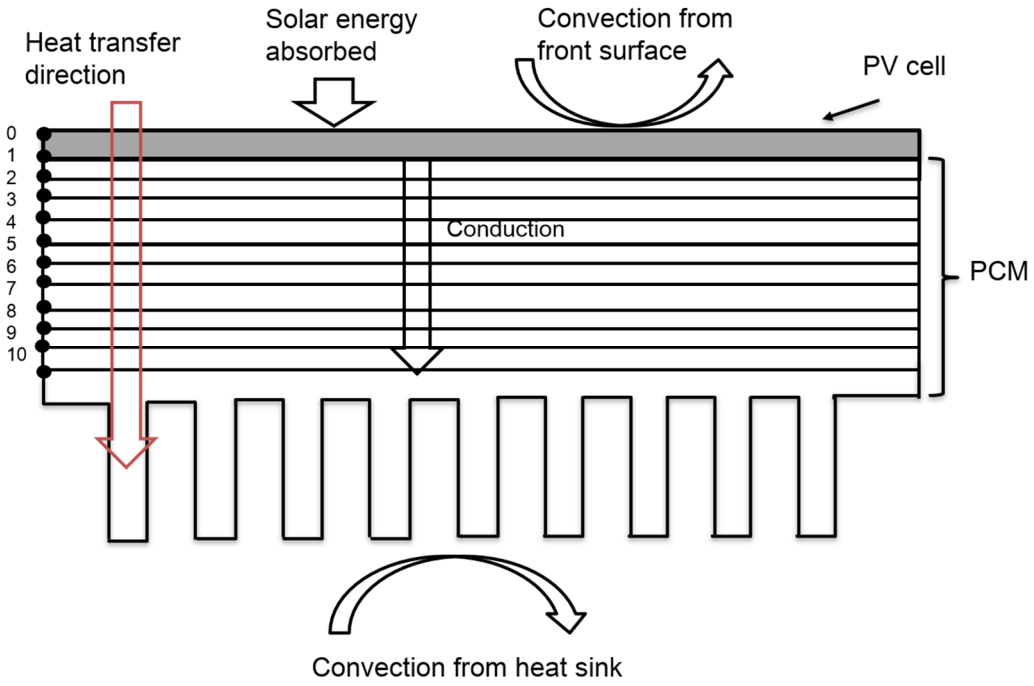

Figure 30 The energy flow scheme of a PV with a finned heat sink. Reproduced with permission from ref. [203], *Copyright (2015) with permission from Elsevier*

The equations used to model the temperatures at all points and the effective specific heat capacity were as follow:

$$\eta Q_{in} = UA(T_0^P - T_\infty) + \rho_{al} V_{al} C_{al} \frac{T_0^{P+\Delta t} - T_0^P}{\Delta t} + \lambda_{al} A \frac{T_0^P - T_1^P}{\Delta x} \quad \text{at point 0} \tag{18}$$

$$\lambda_{al} A \frac{T_0^P - T_1^P}{\Delta x} = \rho_{PCM} V_1 C_{PCM} \frac{T_1^{P+\Delta t} - T_1^P}{\Delta t} + \lambda_{PCM} A \frac{T_1^P - T_2^P}{\Delta x} \quad \text{at point 1} \tag{19}$$

$$\lambda_{PCM} A \frac{T_{n-1}^P - T_n^P}{\Delta x_{(n-1)-n}} = \rho_{PCM} V_n C_{PCM} \frac{T_n^{P+\Delta t} - T_n^P}{\Delta t} + \lambda_{PCM} A \frac{T_n^P - T_{n+1}^P}{\Delta x_{n-(n+1)}} \quad \text{for points 2 to 9} \tag{20}$$

$$\lambda_{PCM} A \frac{T_9^P - T_{10}^P}{\Delta x_{9-10}} = \rho_{PCM} V_n C_{PCM} \frac{T_n^{P+\Delta t} - T_n^P}{\Delta t} + UA_f \, \eta_f (T_{10}^P - T_\infty) \quad \text{at point 10} \tag{21}$$

$$\begin{cases} C = C_{p0} & if\ T \le T_{m1}\ and\ T > T_{m2} \\ C = C_{p0} + \frac{4\Delta H - 4C_{p0}(T_{m1} - T_{m2})}{(T_{m1} - T_{m2})^2} (T - T_{m1}) & if\ T_{m1} < T \le \frac{T_{m1} + T_{m2}}{2} \\ C = C_{p0} + \frac{4\Delta H - 4C_{p0}(T_{m2} - T_{m1})}{(T_{m1} - T_{m2})^2} (T_{m2} - T) & if\ \frac{T_{m1} + T_{m2}}{2} < T \le T_{m2} \end{cases} \tag{22}$$

where Q_{in} stands for the solar radiation, η is the solar absorptance, A and A_f are the cross-section area and the surface area of fins, respectively, η_f is the fin efficiency, T_n^P and T_∞ are respectively the solar panel temperature and the environment temperature. T_{m1} and T_{m2} are respectively the temperature at the beginning of the melting process and the end of the process. Equation (18) was used to calculate the temperature at point 0, equation (19) at point 1, equation (20) at points 2 to 9 and equation (*21*) at point 10. The researcher assumed that the heat transfer is unidirectional, the thermal conductivity and the density are constant and the heat sink is in perfect contact with the solar panel and the PCM. A similar study was done by Zhang *et al.* [203]. They proposed a combination of heat pipes with fins and copper foam to investigate its performance by using the effective heat capacity method and the thermal resistance network. In the same way, Hu *et al.* [204] simulated numerically the thermal behavior of a PCM infiltrated with metallic foam having low porosity. The researcher solved the continuity, energy and momentum equations by using CFD Fluent 18.0 package. The metal-based additives revealed excellent thermal conductivity enhancement. It was noticed by comparing the types of metal additives that the foam could improve the conductivity better than the other types owing to its high porosity and low density.

7.2.2. ***PCM with carbon-based additives***

Carbon-based additives such as graphite, graphene, carbon fiber and carbon nanotube, with their different morphology and microscopic structure, have been used owing to their high thermal conductivity, their low density and their chemical stability [205]. Ling *et al.* [206] studied an organic PCM by using expanded graphite. The thermal conductivity of the composite was predicted by applying a simple equation based on the bulk density and the expanded graphite mass fraction at the ambient temperature. The final equation for the effective thermal conductivity used in the model reads as follow:

$$\lambda_{eff} = \frac{\lambda_G \rho_C \varphi}{\rho_G} \tag{23}$$

where λ_G is the thermal conductivity of the graphite, φ is the mass fraction of the graphite, ρ_C and ρ_G are the bulk density of the composite and the graphite, respectively. Besides, experimental work was achieved to characterize the material with 25% and 35% content of graphite and to validate the numerical model. Results showed that the thermal conductivity of the composite with 35% of graphite is greater by 30% than the composite with 25% of

graphite. This model can be applied to low thermal conductivity PCM with expanded composites.

Elgafi *et al.* [102] also numerically estimated the thermal conductivity of a carbon nanofibers PCM composite and validated the results with an experiment. The analytical model was based on a one-dimensional heat conduction process for a material with low conductivity. Several assumptions were considered such as the uniform distribution of the fibers in the PCM (Figure 31a). The unit cell with symmetry consideration consists of three layers as shown in Figure 31b. The first (I) was composed of PCM and two carbon nanofibers. The second (II) was composed of pure PCM and the third (III) was filled with one carbon nanofiber and PCM. The CNFs are cylinders that have an average outer diameter, D_o, inner diameter, D_i, and length L. Also, it is assumed that $D_i = D_o/4$ and the inner space of the CNFs is filled with air. the CNFs are perpendicular to each other and separated by a distance $D = D_o/4$ from their perpendicular ends and by a distance $d_p = (L + 3D_o/2)$ between their axial axis. The effective thermal conductivity of the material was estimated as the resultant of the thermal conductivities of the three layers. The final equation of the model is as follow:

$$\lambda_{eff} = \frac{2\,\lambda_I\lambda_{II}\lambda_{III}}{2\frac{D_0}{d_p}\lambda_{II}\lambda_{III}+\frac{D_0}{d_p}\lambda_I\lambda_{III}+(2-3\frac{D_0}{d_p})\lambda_I\lambda_{II}} \quad (24)$$

The model's findings were in strong agreement with the results of the experiments. During the study, it was noticed that the thermal conductivity of the tested composite was enhanced since the cooling rate was increased.

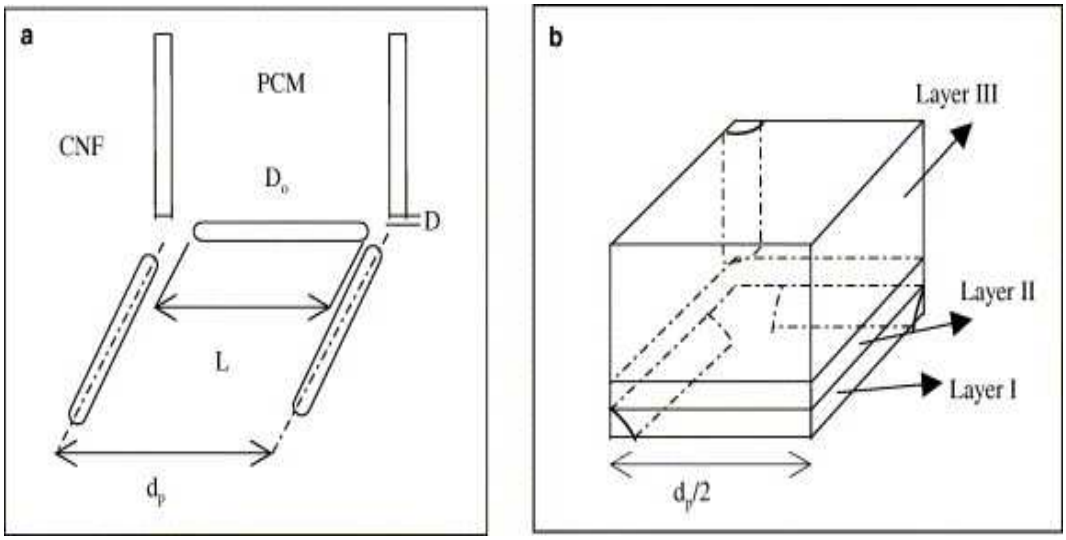

Figure 31 (a) Carbon nanofibers distribution of the composite cell (b) and model of the unit cell. Reproduced with permission from ref. [102]*, Copyright (2015) with permission from Elsevier*

Shaikh *et al.* [130] formulated a mathematical model as presented in equation (25), to calculate the latent energy of the carbon nanotubes, multiwall CNT and carbon nanofibers composites. As a first step, the researchers calculated the interaction between the PCM molecules and the carbon nanoparticles by using Matlab software as an equation solver. Then, a study was carried out to estimate the latent energy of the composite material as a function of the volume fraction of its components.

$$Q = m_{PCM}L + m_{carbon}\Delta H_{max} \quad (25)$$

where Q is the total latent energy, L is the latent heat of the PCM, m_{PCM} and m_{carbon} are the mass of the PCM and the carbon nanoparticles, respectively, and ΔH_{max} is maximum heat capacity. The findings concerning the latent energy determined by using the analytical model agreed well with the experimental results. This theoretical study proves the theory of interaction between particles that can affect the latent heat of the PCM composite. The model can be used for all types of carbon nanoparticle additives. Kant *et al.* [31] investigated the melting of graphene dispersed PCM in an aluminum cavity. Three distinct volume fractions of graphene 1%, 3%, and 5% were considered. The effective thermal conductivity was believed to be the sum of thermal conductivity due to the Brownian motion of nanoparticles and thermal conductivity due to stagnation. The considered equations were solved by using the heat transfer and fluid flow module of COMSOL software. The thermal conductivity of

the graphene/PCM hybrid was increased with the three different volume fractions, resulting in improved heat flow in the cavity. Li *et al.* [207] used the T-history method [208] to determine the thermophysical properties of a paraffin-based composite PCM with different concentrations of graphite. The model is expressed by the following equations that can give the effective specific heat, thermal conductivity, and latent heat:

$$C_S = \left(\frac{m_0 C_0 + m_w C_w}{m_{PCM}}\right) \times \left(\frac{A_3}{A_2}\right) - \frac{m_0}{m_{PCM}} C_0 \quad (26)$$

$$C_L = \left(\frac{m_0 C_0 + m_w C_w}{m_{PCM}}\right) \times \left(\frac{A_1}{A_0}\right) - \frac{m_0}{m_{PCM}} C_0 \quad (27)$$

$$\lambda_s = \frac{1}{1+\frac{C_S(Tm-T\infty)}{L}} \times \frac{025}{\frac{t_f(Tm-T\infty)}{\rho R^2 L} - \frac{1}{2hR}} \quad (28)$$

$$L = \left(\frac{m_0 C_0 + m_w C_w}{m_{PCM}}\right) \times \left(\frac{A_2}{A_0}\right) \times (T_0 - T_{m1}) - \frac{m_0 C_0 (T_{m1} - T_{m2})}{m_{PCM}} \quad (29)$$

where T_0 is the initial temperature, m_0 and m_w are respectively, the mass of the tube filled with the composite PCM and the water mass. *R* is the radius of the tube, t_f is the time of the solidification. *A* is the area of the different regions surrounded by the cooling curve as shown in Figure 32. The findings of the numerical model were in agreement with the experimental results.

From the recent studies, it is clear that carbon-based additives can improve the conductivity of the PCM. However, studies showed that the thermal properties of the carbon additives depend on their aspect ratio. Moreover, the carbon-based additives geometry, density and the method of preparation of the carbon-based composites can also affect the thermal properties of the ensemble.

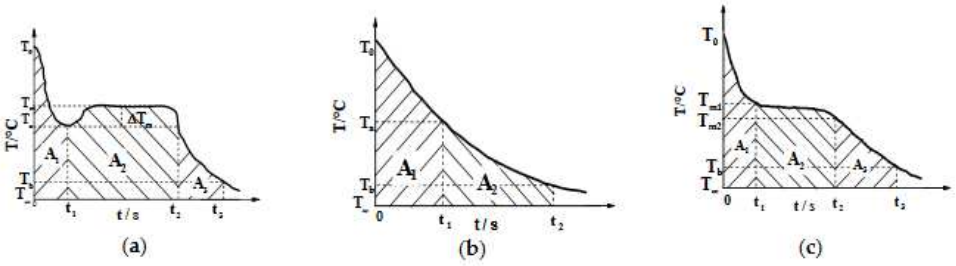

Figure 32 Surrounding region areas A of three PCM cooling curves with (a) supercooling, (b) water and (c) without supercooling. Permission not required [207].

8. Outlook

To date, extensive research has been conducted worldwide to improve the thermophysical properties of PCM in order to promote its use as an efficient thermal energy storage medium. Overall, the findings of the literature review revealed that improving the thermophysical properties of PCM improves the thermal performance of energy storage devices. Several critical issues, however, were identified, including the selection of appropriate additives and concentrations that could meet all of the desired properties. According to the findings, when non-carbon-based additives are added to improve the thermal conductivity of composite PCM, the latent heat of fusion decreases for the same volume of PCM. This improves heat transfer for faster PCM charging and discharging, but decreases the amount of thermal energy stored during the melting of the composite PCM, resulting in a larger container volume for the same amount of thermal energy storage. As a result, using graphene and other carbon-based additives, new ways to develop PCM with improved thermal conductivity and thermal energy storage capacity and minimum supercooling and phase segregation have recently been investigated. Preparing a composite PCM with graphene, for example, is one of the novel concepts to continue to investigate. The advantages of using this additive are the thermal conductivity increase and the latent heat of fusion expansion. Composite PCM are produced and tested for different on-ground applications like electronics cooling, buildings envelop, energy storage reservoirs, heat exchangers, PV panels, etc., and underground geo-structures like heaps, retaining walls, raft foundations, etc. Besides, Repeated cycles of PCM melting and solidification may cause mechanical fatigue on the metallic or carbon-based structures integrated with composite PCM due to the repeated thermal stresses. New research should provide insight into the fluid-structure interactions within such materials.

9. Conclusion

The efficiency of a phase change thermal energy storage device is directly related to its thermophysical properties. The present paper provides a detailed description of PCM thermophysical properties enhancement. The enhancement of thermal conductivity, specific heat and latent heat of fusion, as well as the reduction in the supercooling and phase segregation are discussed. Based on the literature the following conclusions has been drawn:

1. To obtain PCM with high thermal conductivity, thermally conductive nano additives can be used. Nano additive dimension (including pore size, morphology and structure), as well as the loading, determine the thermal conductivity of the resulting composite PCM. Besides, the use of nano additives with anisotropic thermal conductivity or the poor mixing of the composite formulation can result in a PCM with anisotropic thermal conductivity. When nano additives establish phonon channels and minimize interfacial thermal resistance, high thermal conductivity may be reached at large nano additive loadings. Because the pore size influences the heat conductivity and form stability of the final composite PCM, the pore size and structure should be optimized further.
2. Limited studies are focused on the heat storage capacity enhancement of PCM. The heat storage capacity of PCM can be improved by using suitable additives in an appropriate proportion. The addition of single and multiwall carbon nanotubes with specific diameters and appropriate proportions enhances the heat storage capacity of PCM. However, inappropriate concentration may lead to the reduction of the heat storage capacity.
3. The degree of supercooling depends on the container shape and size, PCM composition, heating and cooling rate, heat transfer area, etc. The supercooling can be reduced by adding additives that promote PCM nucleation, by increasing the volume of the PCM container and by avoiding the overheating of the PCM. Reducing the cooling rate may decrease the supercooling degree but increase the time spent in a supercooled state.
4. Phase segregation is bound to happen in PC mixture with different thermophysical properties (density, melting temperature, etc.) Phase segregation may be reduced by increasing the homogeneity of the PCM mixture, by using thickening agents, and by reducing the PCM cooling rate.
5. Various mathematical modelling methods for pure and composite PCM are proposed that can be applied to numerically investigate their thermal behavior and energy storage performance.

Over the past few decades, a great deal of experimental and analytical work has been undertaken, resulting in significant improvements towards reliable and cost-effective PCM. Doping, grafting, or incorporating uniquely structured materials improves the thermal conductivity, sensible heat, and latent heat of fusion of pure PCM. The thermal and chemical stability of such engineered composites must be further assessed before practical use. Novel blends of pure PCM and additives are being developed for the use of thermal energy storage.

This is a very fascinating and important research area currently. The majority of methods for improving PCM properties, production, and cost-effectiveness are still in the testing stage, even though the findings suggest that they are very promising for the thermal energy storage industry.

Nomenclature

A	Cross-sectional area [m^2]
A_f	The cross-sectional area of the fins [m^2]
C_0	Thermal capacity of the tube [J/(kg.K)]
C_w	The thermal capacity of the water [J/(kg.K)]
C_S	The heat capacity in solid-phase [J/(kg.K)]
C_L	The heat capacity in the liquid phase [J/(kg.K)]
C_{al}	The thermal capacity of the aluminum [J/(kg.K)]
f	Number of molecules
f^{eq}	Equilibrium distribution function
f_L	The liquid fraction (%)
h	Enthalpy [J]
$H(T)$	The total enthalpy function [J]
L	The Latent heat (J/kg)
m_{PCM}	Mass of the PCM material [kg]
m_{carbon}	Mass of the carbon nanoparticles [kg]
m_0	The tube mass [kg]
m_w	The water mass [kg]
n	The unit normal vector on the interface
$\dot{q}_{p-f}(t)$	Heat flux on the paraffin cell boundary [W/m^2]
$\dot{q}_{v,s}$	The source term in solid-phase [W/m]
$\dot{q}_{v,L}$	The source term in solid-phase [W/m]

1066	Q	Total latent energy [J]
1067	Q_{in}	Solar energy [J]
1068	R	Radius of the tube [m]
1069	T_S	PCM temperature in solid-phase [K]
1070	T_L	PCM temperature in the liquid phase [K]
1071	T_m	Melting temperature [K]
1072	T^*	Scaled temperature [K]
1073	T_f	Foam temperature [K]
1074	T_{m1}	The temperature at the beginning of the melting phase [K]
1075	T_{m2}	The temperature at the end of the melting phase [K]
1076	T_{PCM}	PCM temperature [K]
1077	T_n^P	Solar panel temperature [K]
1078	T_∞	Environment temperature [K]
1079	T_0	Initial temperature [K]
1080	t_f	Time of solidification [s]
1081	u	Velocity in x direction [m/s]
1082	U	Heat transfer coefficient [W/(K.m^2)]
1083	v	Velocity in y-direction [m/s]
1084	V_{al}	The volume of the aluminum [m^3]
1085	η	Solar Absorptance
1086	η_f	The fin efficiency [%]
1087	$\frac{d\overline{X}}{dt}$	The velocity [m/s]

1088	ρ	The density [kg/m^3]
1089	ρ_{al}	The density of the aluminum [kg/m^3]
1090	ρ_C	Composite density [kg/m^3]
1091	ρ_G	Graphite density [kg/m^3]
1092	λ_{eff}	Effective thermal conductivity [W/(K.m)]
1093	λ_{al}	Thermal conductivity of the aluminum [W/(K.m)]
1094	λ_L	The thermal conductivity in the liquid phase [W/(K.m)]
1095	λ_S	The thermal conductivity in solid-phase [W/(K.m)]
1096	β	The thermal expansion coefficient [1/K]
1097	μ	Dynamic viscosity [kg/(m.s)]
1098	Ω	Integrodifferential factor
1099	CF	Carbon fiber
1100	CNF	Carbon nanofiber
1101	CNT	Carbon nanotubes
1102	MWCNT	Multiwall carbon nanotubes
1103	NDG	Nitrogen-doped graphene
1104	SWCNT	Single-wall carbon nanotubes
1105		
1106		

References

[1] Y. Shimoda, Y. Yamaguchi, Y. Iwafune, K. Hidaka, A. Meier, Y. Yagita, H. Kawamoto, S. Nishikiori, Energy demand science for a decarbonized society in the context of the residential sector, Renewable and Sustainable Energy Reviews. 132 (2020) 110051. https://doi.org/10.1016/j.rser.2020.110051.

[2] T. Ahmad, D. Zhang, A critical review of comparative global historical energy consumption and future demand: The story told so far, Energy Reports. 6 (2020) 1973–1991. https://doi.org/10.1016/j.egyr.2020.07.020.

[3] D. Mariano-Hernández, L. Hernández-Callejo, A. Zorita-Lamadrid, O. Duque-Pérez, F. Santos García, A review of strategies for building energy management system: Model predictive control, demand side management, optimization, and fault detect & diagnosis, Journal of Building Engineering. 33 (2021) 101692. https://doi.org/10.1016/j.jobe.2020.101692.

[4] A. Sharma, A. Shukla, K. Kant, Perspective of Solar Energy in India, in: Green Energy and Technology, 2018: pp. 17–35. https://doi.org/10.1007/978-981-10-7326-7_2.

[5] K. Nithyanandam, J. Stekli, R. Pitchumani, High-temperature latent heat storage for concentrating solar thermal (CST) systems, in: Advances in Concentrating Solar Thermal Research and Technology, 2017: pp. 213–246. https://doi.org/10.1016/B978-0-08-100516-3.00010-1.

[6] K. Kant, A. Shukla, A. Sharma, P.H. Biwole, Heat transfer studies of photovoltaic panel coupled with phase change material, Solar Energy. 140 (2016) 151–161. https://doi.org/10.1016/j.solener.2016.11.006.

[7] K. Kant, A. Anand, A. Shukla, A. Sharma, Heat transfer study of building integrated photovoltaic (BIPV) with nano-enhanced phase change materials, Journal of Energy Storage. 30 (2020) 101563. https://doi.org/10.1016/j.est.2020.101563.

[8] F. Souayfane, F. Fardoun, P.-H. Biwole, Phase change materials (PCM) for cooling applications in buildings: A review, Energy and Buildings. 129 (2016) 396–431. https://doi.org/10.1016/j.enbuild.2016.04.006.

[9] L. Ianniciello, P.H. Biwolé, P. Achard, Electric vehicles batteries thermal management systems employing phase change materials, Journal of Power Sources. 378 (2018) 383–403. https://doi.org/10.1016/j.jpowsour.2017.12.071.

[10] S.Y. Kee, Y. Munusamy, K.S. Ong, Review of solar water heaters incorporating solid-liquid organic phase change materials as thermal storage, Applied Thermal Engineering. 131 (2018) 455–471. https://doi.org/10.1016/j.applthermaleng.2017.12.032.

[11] A. Sharma, V.V. Tyagi, C.R. Chen, D. Buddhi, Review on thermal energy storage with phase change materials and applications, Renewable and Sustainable Energy Reviews. 13 (2009) 318–345. https://doi.org/10.1016/j.rser.2007.10.005.

[12] A. Shukla, K. Kant, A. Sharma, Solar still with latent heat energy storage: A review, Innovative Food Science and Emerging Technologies. 41 (2017) 34–46. https://doi.org/10.1016/j.csl.2006.06.005.

[13] A. Fallahi, G. Guldentops, M. Tao, S. Granados-Focil, S. Van Dessel, Review on solid-solid phase change materials for thermal energy storage: Molecular structure and thermal properties, Applied Thermal Engineering. 127 (2017) 1427–1441. https://doi.org/10.1016/j.applthermaleng.2017.08.161.

[14] H. Benli, A. Durmuş, Performance analysis of a latent heat storage system with phase change material for new designed solar collectors in greenhouse heating, Solar Energy. 83 (2009) 2109–2119. https://doi.org/10.1016/j.solener.2009.07.005.

[15] S. Kooli, S. Bouadila, M. Lazaar, A. Farhat, The effect of nocturnal shutter on insulated greenhouse using a solar air heater with latent storage energy, Solar Energy. 115 (2015) 217–228. https://doi.org/10.1016/j.solener.2015.02.041.

[16] S. Gorjian, F. Calise, K. Kant, M.S. Ahamed, B. Copertaro, G. Najafi, X. Zhang, M. Aghaei, R.R. Shamshiri, A review on opportunities for implementation of solar energy technologies in agricultural greenhouses, Journal of Cleaner Production. 285 (2021) 124807. https://doi.org/10.1016/j.jclepro.2020.124807.

[17] A.H.A. Al-Waeli, K. Sopian, M.T. Chaichan, H.A. Kazem, A. Ibrahim, S. Mat, M.H. Ruslan, Evaluation of the nanofluid and nano-PCM based photovoltaic thermal (PVT) system: An experimental study, Energy Conversion and Management. 151 (2017) 693–708. https://doi.org/10.1016/j.enconman.2017.09.032.

[18] Z. Luo, Z. Huang, N. Xie, X. Gao, T. Xu, Y. Fang, Z. Zhang, Numerical and experimental study on temperature control of solar panels with form-stable paraffin/expanded graphite composite PCM, Energy Conversion and Management. (2017). https://doi.org/10.1016/j.enconman.2017.07.046.

[19] R. M., L. S., R. S., A. H., D. A., Experimental investigation on the abasement of operating temperature in solar photovoltaic panel using PCM and aluminium, Solar Energy. 188 (2019) 327–338. https://doi.org/10.1016/j.solener.2019.05.067.

[20] A.A.M. Omara, A.A.A. Abuelnuor, Trombe walls with phase change materials: A review, Energy Storage. (2020). https://doi.org/10.1002/est2.123.

[21] X. Kong, L. Wang, H. Li, G. Yuan, C. Yao, Experimental study on a novel hybrid system of active composite PCM wall and solar thermal system for clean heating supply in winter, Solar Energy. (2020). https://doi.org/10.1016/j.solener.2019.11.081.

[22] E. Tunçbilek, M. Arıcı, M. Krajčík, S. Nižetić, H. Karabay, Thermal performance based optimization of an office wall containing PCM under intermittent cooling operation, Applied Thermal Engineering. (2020). https://doi.org/10.1016/j.applthermaleng.2020.115750.

[23] S. Zhang, W. Hu, D. Li, C. Zhang, M. Arıcı, Ç. Yıldız, X. Zhang, Y. Ma, Energy efficiency optimization of PCM and aerogel-filled multiple glazing windows, Energy. (2021). https://doi.org/10.1016/j.energy.2021.119916.

[24] C. Yan, W. Shi, X. Li, S. Wang, A seasonal cold storage system based on separate type heat pipe for sustainable building cooling, Renewable Energy. (2016). https://doi.org/10.1016/j.renene.2015.07.023.

[25] M. Luo, J. Song, Z. Ling, Z. Zhang, X. Fang, Phase Change Material (PCM) coat for battery thermal management with integrated rapid heating and cooling functions from -40 °C to 50 °C, Materials Today Energy. (2021) 100652. https://doi.org/10.1016/j.mtener.2021.100652.

[26] A. Desai, V.K. Singh, R.R. Bhavsar, NUMERICAL INVESTIGATION OF PCM BASED THERMAL CONTROL MODULE FOR SPACE APPLICATIONS, in: Proceeding of Proceedings of the 24th National and 2nd International ISHMT-ASTFE Heat and Mass Transfer Conference (IHMTC-2017), Begellhouse, Connecticut, 2018: pp. 621–628. https://doi.org/10.1615/IHMTC-2017.870.

[27] A.N. Desai, A. Gunjal, V.K. Singh, Numerical investigations of fin efficacy for phase change material (PCM) based thermal control module, International Journal of Heat and Mass Transfer. 147 (2020) 118855. https://doi.org/10.1016/j.ijheatmasstransfer.2019.118855.

[28] K. Kant, A. Shukla, A. Sharma, Advancement in phase change materials for thermal energy storage applications, Solar Energy Materials and Solar Cells. 172 (2017) 82–92. https://doi.org/10.1016/j.solmat.2017.07.023.

[29] P. Cheng, X. Chen, H. Gao, X. Zhang, Z. Tang, A. Li, G. Wang, Different dimensional nanoadditives for thermal conductivity enhancement of phase change materials: Fundamentals and applications, Nano Energy. 85 (2021) 105948. https://doi.org/10.1016/j.nanoen.2021.105948.

[30] B. Li, X. Zhai, X. Cheng, Experimental and numerical investigation of a solar collector/storage system with composite phase change materials, Solar Energy. 164 (2018) 65–76. https://doi.org/10.1016/j.solener.2018.02.031.

[31] K. Kant, A. Shukla, A. Sharma, P. Henry Biwole, Heat transfer study of phase change materials with graphene nano particle for thermal energy storage, Solar Energy. 146 (2017) 453–463. https://doi.org/10.1016/j.solener.2017.03.013.

[32] S. Wu, T. Yan, Z. Kuai, W. Pan, Thermal conductivity enhancement on phase change materials for thermal energy storage: A review, Energy Storage Materials. 25 (2020) 251–295. https://doi.org/10.1016/j.ensm.2019.10.010.

[33] R. Singh, S. Sadeghi, B. Shabani, Thermal Conductivity Enhancement of Phase Change Materials for Low-Temperature Thermal Energy Storage Applications, Energies. 12 (2018) 75. https://doi.org/10.3390/en12010075.

[34] N. Mehra, L. Mu, T. Ji, X. Yang, J. Kong, J. Gu, J. Zhu, Thermal transport in polymeric materials and across composite interfaces, Applied Materials Today. 12 (2018) 92–130. https://doi.org/10.1016/j.apmt.2018.04.004.

[35] J. Maire, R. Anufriev, R. Yanagisawa, A. Ramiere, S. Volz, M. Nomura, Heat conduction tuning by wave nature of phonons, Science Advances. 3 (2017) 1–7. https://doi.org/10.1126/sciadv.1700027.

[36] Von N. W. Ashcroft; N. D. Mermin, Solid State Physics. , New York 1976, XXII, 826 Seiten, 1976.

[37] C. Kittel, Introduction to Solid State Physics, 8th edition, Wiley & Sons, New York, NY. (2004).

[38] A.J. Minnich, Advances in the measurement and computation of thermal phonon transport properties, Journal of Physics: Condensed Matter. 27 (2015) 053202.

https://doi.org/10.1088/0953-8984/27/5/053202.

[39] W.S. Capinski, H.J. Maris, T. Ruf, M. Cardona, K. Ploog, D.S. Katzer, Thermal-conductivity measurements of GaAs/AlAs superlattices using a picosecond optical pump-and-probe technique, Physical Review B. 59 (1999) 8105–8113. https://doi.org/10.1103/PhysRevB.59.8105.

[40] D.G. Atinafu, W. Dong, X. Huang, H. Gao, G. Wang, Introduction of organic-organic eutectic PCM in mesoporous N-doped carbons for enhanced thermal conductivity and energy storage capacity, Applied Energy. 211 (2018) 1203–1215. https://doi.org/10.1016/j.apenergy.2017.12.025.

[41] M. Mehrali, S. Tahan Latibari, M. Mehrali, T.M.I. Mahlia, E. Sadeghinezhad, H.S.C. Metselaar, Preparation of nitrogen-doped graphene/palmitic acid shape stabilized composite phase change material with remarkable thermal properties for thermal energy storage, Applied Energy. 135 (2014) 339–349. https://doi.org/10.1016/j.apenergy.2014.08.100.

[42] X. Chen, H. Gao, L. Xing, W. Dong, A. Li, P. Cheng, P. Liu, G. Wang, Nanoconfinement effects of N-doped hierarchical carbon on thermal behaviors of organic phase change materials, Energy Storage Materials. 18 (2019) 280–288. https://doi.org/10.1016/j.ensm.2018.08.024.

[43] D.G. Atinafu, W. Dong, C. Hou, R.S. Andriamitantsoa, J. Wang, X. Huang, H. Gao, G. Wang, A facile one-step synthesis of porous N-doped carbon from MOF for efficient thermal energy storage capacity of shape-stabilized phase change materials, Materials Today Energy. 12 (2019) 239–249. https://doi.org/10.1016/j.mtener.2019.01.011.

[44] J. Wang, X. Huang, H. Gao, A. Li, C. Wang, Construction of CNT@Cr-MIL-101-NH2 hybrid composite for shape-stabilized phase change materials with enhanced thermal conductivity, Chemical Engineering Journal. 350 (2018) 164–172. https://doi.org/10.1016/j.cej.2018.05.190.

[45] M. Li, M. Chen, Z. Wu, J. Liu, Carbon nanotube grafted with polyalcohol and its influence on the thermal conductivity of phase change material, Energy Conversion and Management. 83 (2014) 325–329. https://doi.org/10.1016/j.enconman.2014.04.002.

[46] D.-Z. Chen, S.-Y. Qin, G.C.P. Tsui, C. Tang, X. Ouyang, J. Liu, J.-N. Tang, J.-D. Zuo,

Fabrication, morphology and thermal properties of octadecylamine-grafted graphene oxide-modified phase-change microcapsules for thermal energy storage, Composites Part B: Engineering. 157 (2019) 239–247. https://doi.org/10.1016/j.compositesb.2018.08.066.

[47] F. Xue, X. Qi, T. Huang, C. Tang, N. Zhang, Y. Wang, Preparation and application of three-dimensional filler network towards organic phase change materials with high performance and multi-functions, Chemical Engineering Journal. 419 (2021) 129620. https://doi.org/10.1016/j.cej.2021.129620.

[48] M.M. Umair, Y. Zhang, K. Iqbal, S. Zhang, B. Tang, Novel strategies and supporting materials applied to shape-stabilize organic phase change materials for thermal energy storage–A review, Applied Energy. 235 (2019) 846–873. https://doi.org/10.1016/j.apenergy.2018.11.017.

[49] H. Ji, D.P. Sellan, M.T. Pettes, X. Kong, J. Ji, L. Shi, R.S. Ruoff, Enhanced thermal conductivity of phase change materials with ultrathin-graphite foams for thermal energy storage, Energy Environ. Sci. 7 (2014) 1185–1192. https://doi.org/10.1039/C3EE42573H.

[50] L. Xia, P. Zhang, R.Z. Wang, Preparation and thermal characterization of expanded graphite/paraffin composite phase change material, Carbon. 48 (2010) 2538–2548. https://doi.org/10.1016/j.carbon.2010.03.030.

[51] X. Xiao, P. Zhang, Morphologies and thermal characterization of paraffin/carbon foam composite phase change material, Solar Energy Materials and Solar Cells. 117 (2013) 451–461. https://doi.org/10.1016/j.solmat.2013.06.037.

[52] M. Karthik, A. Faik, P. Blanco-Rodríguez, J. Rodríguez-Aseguinolaza, B. D'Aguanno, Preparation of erythritol–graphite foam phase change composite with enhanced thermal conductivity for thermal energy storage applications, Carbon. 94 (2015) 266–276. https://doi.org/10.1016/j.carbon.2015.06.075.

[53] M. Karthik, A. Faik, B. D'Aguanno, Graphite foam as interpenetrating matrices for phase change paraffin wax: A candidate composite for low temperature thermal energy storage, Solar Energy Materials and Solar Cells. 172 (2017) 324–334. https://doi.org/10.1016/j.solmat.2017.08.004.

[54] L. Zhang, K. Zhou, Q. Wei, L. Ma, W. Ye, H. Li, B. Zhou, Z. Yu, C.-T. Lin, J. Luo, X. Gan, Thermal conductivity enhancement of phase change materials with 3D porous

diamond foam for thermal energy storage, Applied Energy. 233–234 (2019) 208–219. https://doi.org/10.1016/j.apenergy.2018.10.036.

[55] W.G. Alshaer, S.A. Nada, M.A. Rady, C. Le Bot, E. Palomo Del Barrio, Numerical investigations of using carbon foam/PCM/Nano carbon tubes composites in thermal management of electronic equipment, Energy Conversion and Management. 89 (2015) 873–884. https://doi.org/10.1016/j.enconman.2014.10.045.

[56] O. Mesalhy, K. Lafdi, A. Elgafy, Carbon foam matrices saturated with PCM for thermal protection purposes, Carbon. 44 (2006) 2080–2088. https://doi.org/10.1016/j.carbon.2005.12.019.

[57] X. Chen, H. Gao, M. Yang, W. Dong, X. Huang, A. Li, C. Dong, G. Wang, Highly graphitized 3D network carbon for shape-stabilized composite PCMs with superior thermal energy harvesting, Nano Energy. 49 (2018) 86–94. https://doi.org/10.1016/j.nanoen.2018.03.075.

[58] C. Amaral, R. Vicente, P.A.A.P. Marques, A. Barros-Timmons, Phase change materials and carbon nanostructures for thermal energy storage: A literature review, Renewable and Sustainable Energy Reviews. 79 (2017) 1212–1228. https://doi.org/10.1016/j.rser.2017.05.093.

[59] A. Li, J. Wang, C. Dong, W. Dong, D.G. Atinafu, X. Chen, H. Gao, G. Wang, Core-sheath structural carbon materials for integrated enhancement of thermal conductivity and capacity, Applied Energy. 217 (2018) 369–376. https://doi.org/10.1016/j.apenergy.2017.12.106.

[60] N. Hu, H. Li, Q. Wei, K. Zhou, W. Zhu, L. Zhang, S. Li, W. Ye, Z. Jiao, J. Luo, L. Ma, Q. Yan, C.-T. Lin, Continuous diamond-carbon nanotube foams as rapid heat conduction channels in composite phase change materials based on the stable hierarchical structure, Composites Part B: Engineering. 200 (2020) 108293. https://doi.org/10.1016/j.compositesb.2020.108293.

[61] I. Kholmanov, J. Kim, E. Ou, R.S. Ruoff, L. Shi, Continuous Carbon Nanotube–Ultrathin Graphite Hybrid Foams for Increased Thermal Conductivity and Suppressed Subcooling in Composite Phase Change Materials, ACS Nano. 9 (2015) 11699–11707. https://doi.org/10.1021/acsnano.5b02917.

[62] J. Yang, E. Zhang, X. Li, Y. Zhang, J. Qu, Z.-Z. Yu, Cellulose/graphene aerogel supported phase change composites with high thermal conductivity and good shape

stability for thermal energy storage, Carbon. 98 (2016) 50–57. https://doi.org/10.1016/j.carbon.2015.10.082.

[63] X. Liu, Z. Rao, Thermal diffusion and phase transition of n-octadecane as thermal energy storage material on nanoscale copper surface: A molecular dynamics study, Journal of the Energy Institute. 92 (2019) 161–176. https://doi.org/10.1016/j.joei.2017.10.011.

[64] C. Wang, T. Lin, N. Li, H. Zheng, Heat transfer enhancement of phase change composite material: Copper foam/paraffin, Renewable Energy. 96 (2016) 960–965. https://doi.org/10.1016/j.renene.2016.04.039.

[65] H. Zheng, C. Wang, Q. Liu, Z. Tian, X. Fan, Thermal performance of copper foam/paraffin composite phase change material, Energy Conversion and Management. 157 (2018) 372–381. https://doi.org/10.1016/j.enconman.2017.12.023.

[66] Z. Wang, Z. Zhang, L. Jia, L. Yang, Paraffin and paraffin/aluminum foam composite phase change material heat storage experimental study based on thermal management of Li-ion battery, Applied Thermal Engineering. 78 (2015) 428–436. https://doi.org/10.1016/j.applthermaleng.2015.01.009.

[67] J. Jiang, Y. Zhu, A. Ma, D. Yang, F. Lu, J. Chen, J. Shi, D. Song, Preparation and performances of bulk porous Al foams impregnated with phase-change-materials for thermal storage, Progress in Natural Science: Materials International. 22 (2012) 440–444. https://doi.org/10.1016/j.pnsc.2012.05.004.

[68] Y. Li, J. Li, Y. Deng, W. Guan, X. Wang, T. Qian, Preparation of paraffin/porous TiO 2 foams with enhanced thermal conductivity as PCM, by covering the TiO 2 surface with a carbon layer, Applied Energy. 171 (2016) 37–45. https://doi.org/10.1016/j.apenergy.2016.03.010.

[69] X. Xiao, P. Zhang, M. Li, Preparation and thermal characterization of paraffin/metal foam composite phase change material, Applied Energy. 112 (2013) 1357–1366. https://doi.org/10.1016/j.apenergy.2013.04.050.

[70] X. Xiao, P. Zhang, M. Li, Effective thermal conductivity of open-cell metal foams impregnated with pure paraffin for latent heat storage, International Journal of Thermal Sciences. 81 (2014) 94–105. https://doi.org/10.1016/j.ijthermalsci.2014.03.006.

[71] T. Oya, T. Nomura, N. Okinaka, T. Akiyama, Phase change composite based on

1359 porous nickel and erythritol, Applied Thermal Engineering. 40 (2012) 373–377.
1360 https://doi.org/10.1016/j.applthermaleng.2012.02.033.

1361 [72] A.R. Abdulmunem, P.M. Samin, H.A. Rahman, H.A. Hussien, H. Ghazali, A novel
1362 thermal regulation method for photovoltaic panels using porous metals filled with
1363 phase change material and nanoparticle additives, Journal of Energy Storage. 39
1364 (2021) 102621. https://doi.org/10.1016/j.est.2021.102621.

1365 [73] A. Sarı, A. Karaipekli, Thermal conductivity and latent heat thermal energy storage
1366 characteristics of paraffin/expanded graphite composite as phase change material,
1367 Applied Thermal Engineering. 27 (2007) 1271–1277.
1368 https://doi.org/10.1016/j.applthermaleng.2006.11.004.

1369 [74] A. Sari, A. Karaipekli, Preparation, thermal properties and thermal reliability of
1370 palmitic acid/expanded graphite composite as form-stable PCM for thermal energy
1371 storage, Solar Energy Materials and Solar Cells. 93 (2009) 571–576.
1372 https://doi.org/10.1016/j.solmat.2008.11.057.

1373 [75] M. Yuan, Y. Ren, C. Xu, F. Ye, X. Du, Characterization and stability study of a form-
1374 stable erythritol/expanded graphite composite phase change material for thermal
1375 energy storage, Renewable Energy. 136 (2019) 211–222.
1376 https://doi.org/10.1016/j.renene.2018.12.107.

1377 [76] A.J.H. McGaughey, M. Kaviany, Thermal conductivity decomposition and analysis
1378 using molecular dynamics simulations, International Journal of Heat and Mass
1379 Transfer. 47 (2004) 1799–1816.
1380 https://doi.org/10.1016/j.ijheatmasstransfer.2003.11.009.

1381 [77] K. Peng, L. Fu, X. Li, J. Ouyang, H. Yang, Stearic acid modified montmorillonite as
1382 emerging microcapsules for thermal energy storage, Applied Clay Science. 138 (2017)
1383 100–106. https://doi.org/10.1016/j.clay.2017.01.003.

1384 [78] Y. Zhou, Y. Bai, K. Yu, Y. Kang, H. Wang, Excellent thermal conductivity and
1385 dielectric properties of polyimide composites filled with silica coated self-passivated
1386 aluminum fibers and nanoparticles, Applied Physics Letters. 102 (2013) 252903.
1387 https://doi.org/10.1063/1.4812653.

1388 [79] W. Fu, X. Liang, H. Xie, S. Wang, X. Gao, Z. Zhang, Y. Fang, Thermophysical
1389 properties of n -tetradecane@polystyrene-silica composite nanoencapsulated phase
1390 change material slurry for cold energy storage, Energy and Buildings. 136 (2017) 26–

1391 32. https://doi.org/10.1016/j.enbuild.2016.12.001.

1392 [80] H. Zhang, X. Wang, D. Wu, Silica encapsulation of n-octadecane via sol–gel process:
1393 A novel microencapsulated phase-change material with enhanced thermal conductivity
1394 and performance, Journal of Colloid and Interface Science. 343 (2010) 246–255.
1395 https://doi.org/10.1016/j.jcis.2009.11.036.

1396 [81] A. Babapoor, G. Karimi, Thermal properties measurement and heat storage analysis of
1397 paraffinnanoparticles composites phase change material: Comparison and
1398 optimization, Applied Thermal Engineering. 90 (2015) 945–951.
1399 https://doi.org/10.1016/j.applthermaleng.2015.07.083.

1400 [82] M. Silakhori, H.S.C. Metselaar, T.M.I. Mahlia, H. Fauzi, S. Baradaran, M.S. Naghavi,
1401 Palmitic acid/polypyrrole composites as form-stable phase change materials for
1402 thermal energy storage, Energy Conversion and Management. 80 (2014) 491–497.
1403 https://doi.org/10.1016/j.enconman.2014.01.023.

1404 [83] A. Karaipekli, A. Sari, A. Sarı, Capric-myristic acid/vermiculite composite as form-
1405 stable phase change material for thermal energy storage, Solar Energy. 83 (2009) 323–
1406 332. https://doi.org/10.1016/j.solener.2008.08.012.

1407 [84] A. Sarı, A. Biçer, Preparation and thermal energy storage properties of building
1408 material-based composites as novel form-stable PCMs, Energy and Buildings. 51
1409 (2012) 73–83. https://doi.org/10.1016/j.enbuild.2012.04.010.

1410 [85] A. Karaipekli, A. Sarı, Preparation and characterization of fatty acid ester/building
1411 material composites for thermal energy storage in buildings, Energy and Buildings. 43
1412 (2011) 1952–1959. https://doi.org/10.1016/j.enbuild.2011.04.002.

1413 [86] A. Sarı, A. Biçer, Thermal energy storage properties and thermal reliability of some
1414 fatty acid esters/building material composites as novel form-stable PCMs, Solar
1415 Energy Materials and Solar Cells. 101 (2012) 114–122.
1416 https://doi.org/10.1016/j.solmat.2012.02.026.

1417 [87] Y. Liu, E. Xu, M. Xie, X. Gao, Y. Yang, H. Deng, Use of calcium silicate-coated
1418 paraffin/expanded perlite materials to improve the thermal performance of cement
1419 mortar, Construction and Building Materials. 189 (2018) 218–226.
1420 https://doi.org/10.1016/j.conbuildmat.2018.08.213.

1421 [88] D. Sun, L. Wang, Utilization of paraffin/expanded perlite materials to improve

mechanical and thermal properties of cement mortar, Construction and Building Materials. 101 (2015) 791–796. https://doi.org/10.1016/j.conbuildmat.2015.10.123.

[89] M. Li, Z. Wu, H. Kao, Study on preparation and thermal properties of binary fatty acid/diatomite shape-stabilized phase change materials, Solar Energy Materials and Solar Cells. 95 (2011) 2412–2416. https://doi.org/10.1016/j.solmat.2011.04.017.

[90] M. Li, H. Kao, Z. Wu, J. Tan, Study on preparation and thermal property of binary fatty acid and the binary fatty acids/diatomite composite phase change materials, Applied Energy. 88 (2011) 1606–1612. https://doi.org/10.1016/j.apenergy.2010.11.001.

[91] S. Song, L. Dong, S. Chen, H. Xie, C. Xiong, Stearic–capric acid eutectic/activated-attapulgiate composite as form-stable phase change material for thermal energy storage, Energy Conversion and Management. 81 (2014) 306–311. https://doi.org/10.1016/j.enconman.2014.02.045.

[92] R. Wen, X. Zhang, Y. Huang, Z. Yin, Z. Huang, M. Fang, Y. Liu, X. Wu, Preparation and properties of fatty acid eutectics/expanded perlite and expanded vermiculite shape-stabilized materials for thermal energy storage in buildings, Energy and Buildings. 139 (2017) 197–204. https://doi.org/10.1016/j.enbuild.2017.01.025.

[93] X. Zhang, Z. Yin, D. Meng, Z. Huang, R. Wen, Y. Huang, X. Min, Y. Liu, M. Fang, X. Wu, Shape-stabilized composite phase change materials with high thermal conductivity based on stearic acid and modified expanded vermiculite, Renewable Energy. 112 (2017) 113–123. https://doi.org/10.1016/j.renene.2017.05.026.

[94] Y. Deng, J.H. Li, T.T. Qian, W.M. Guan, X. Wang, Polyethylene Glycol/Expanded Vermiculite Shape-Stabilized Composite Phase Change Materials for Thermal Energy Storage, Materials Science Forum. 847 (2016) 39–45. https://doi.org/10.4028/www.scientific.net/MSF.847.39.

[95] S. Xu, X. Zhang, Z. Huang, Y. Liu, M. Fang, X. Wu, X. Min, Thermal conductivity enhanced polyethylene glycol/expanded perlite shape-stabilized composite phase change materials with Cu powder for thermal energy storage, Materials Research Express. 5 (2018) 095503. https://doi.org/10.1088/2053-1591/aad5c0.

[96] Y. Deng, J. Li, H. Nian, Polyethylene glycol-enwrapped silicon carbide nanowires network/expanded vermiculite composite phase change materials: Form-stabilization, thermal energy storage behavior and thermal conductivity enhancement, Solar Energy

Materials and Solar Cells. 174 (2018) 283–291. https://doi.org/10.1016/j.solmat.2017.09.013.

[97] Y. Deng, J. Li, T. Qian, W. Guan, Y. Li, X. Yin, Thermal conductivity enhancement of polyethylene glycol/expanded vermiculite shape-stabilized composite phase change materials with silver nanowire for thermal energy storage, Chemical Engineering Journal. 295 (2016) 427–435. https://doi.org/10.1016/j.cej.2016.03.068.

[98] X. Jin, Q. Xiao, T. Xu, G. Huang, H. Wu, D. Wang, Y. Liu, H. Zhang, A.C.K. Lai, Thermal conductivity enhancement of a sodium acetate trihydrate–potassium chloride–urea/expanded graphite composite phase–change material for latent heat thermal energy storage, Energy and Buildings. 231 (2021) 110615. https://doi.org/10.1016/j.enbuild.2020.110615.

[99] G. Ma, J. Sun, Y. Zhang, Y. Jing, Y. Jia, Preparation and thermal properties of stearic acid-benzamide eutectic mixture/expanded graphite composites as phase change materials for thermal energy storage, Powder Technology. 342 (2019) 131–140. https://doi.org/10.1016/j.powtec.2018.09.074.

[100] P.K. Singh Rathore, S. kumar Shukla, Improvement in thermal properties of PCM/Expanded Vermiculite/Expanded Graphite shape stabilized composite PCM for building energy applications, Renewable Energy. (2021). https://doi.org/10.1016/j.renene.2021.05.068.

[101] J. Fukai, M. Kanou, Y. Kodama, O. Miyatake, Thermal conductivity enhancement of energy storage media using carbon fibers, Energy Convers. Manag. 41 (2000) 1543–1556. https://doi.org/10.1016/S0196-8904(99)00166-1.

[102] A. Elgafy, K. Lafdi, Effect of carbon nanofiber additives on thermal behavior of phase change materials, Carbon. 43 (2005) 3067–3074. https://doi.org/10.1016/j.carbon.2005.06.042.

[103] Z. Jiang, T. Ouyang, Y. Yang, L. Chen, X. Fan, Y. Chen, W. Li, Y. Fei, Thermal conductivity enhancement of phase change materials with form-stable carbon bonded carbon fiber network, Materials & Design. 143 (2018) 177–184. https://doi.org/10.1016/j.matdes.2018.01.052.

[104] T. Qian, J. Li, W. Feng, H. Nian, Single-walled carbon nanotube for shape stabilization and enhanced phase change heat transfer of polyethylene glycol phase change material, Energy Conversion and Management. 143 (2017) 96–108.

https://doi.org/10.1016/j.enconman.2017.03.065.

[105] X. Chen, H. Gao, G. Hai, D. Jia, L. Xing, S. Chen, P. Cheng, M. Han, W. Dong, G. Wang, Carbon nanotube bundles assembled flexible hierarchical framework based phase change material composites for thermal energy harvesting and thermotherapy, Energy Storage Materials. 26 (2020) 129–137. https://doi.org/10.1016/j.ensm.2019.12.029.

[106] P. Cheng, H. Gao, X. Chen, Y. Chen, M. Han, L. Xing, P. Liu, G. Wang, Flexible monolithic phase change material based on carbon nanotubes/chitosan/poly(vinyl alcohol), Chemical Engineering Journal. 397 (2020) 125330. https://doi.org/10.1016/j.cej.2020.125330.

[107] F. Bahiraei, A. Fartaj, G.A. Nazri, Experimental and numerical investigation on the performance of carbon-based nanoenhanced phase change materials for thermal management applications, Energy Conversion and Management. (2017). https://doi.org/10.1016/j.enconman.2017.09.065.

[108] S. Sami, N. Etesami, Improving thermal characteristics and stability of phase change material containing TiO2 nanoparticles after thermal cycles for energy storage, Applied Thermal Engineering. (2017). https://doi.org/10.1016/j.applthermaleng.2017.06.023.

[109] J. Wang, H. Xie, Z. Guo, L. Guan, Y. Li, Improved thermal properties of paraffin wax by the addition of TiO2 nanoparticles, Applied Thermal Engineering. (2014). https://doi.org/10.1016/j.applthermaleng.2014.05.078.

[110] F. Tang, L. Cao, G. Fang, Preparation and thermal properties of stearic acid/titanium dioxide composites as shape-stabilized phase change materials for building thermal energy storage, Energy and Buildings. 80 (2014) 352–357. https://doi.org/10.1016/j.enbuild.2014.05.030.

[111] R.M. Al Ghossein, M.S. Hossain, J.M. Khodadadi, Experimental determination of temperature-dependent thermal conductivity of solid eicosane-based silver nanostructure-enhanced phase change materials for thermal energy storage, International Journal of Heat and Mass Transfer. (2017). https://doi.org/10.1016/j.ijheatmasstransfer.2016.11.059.

[112] Y. Yang, J. Luo, G. Song, Y. Liu, G. Tang, The experimental exploration of nano-Si3N4/paraffin on thermal behavior of phase change materials, Thermochimica Acta.

(2014). https://doi.org/10.1016/j.tca.2014.10.014.

[113] W. Han, C. Ge, R. Zhang, Z. Ma, L. Wang, X. Zhang, Boron nitride foam as a polymer alternative in packaging phase change materials: Synthesis, thermal properties and shape stability, Applied Energy. (2019). https://doi.org/10.1016/j.apenergy.2019.01.153.

[114] Z. Qian, H. Shen, X. Fang, L. Fan, N. Zhao, J. Xu, Phase change materials of paraffin in h-BN porous scaffolds with enhanced thermal conductivity and form stability, Energy and Buildings. (2018). https://doi.org/10.1016/j.enbuild.2017.11.033.

[115] J. Yang, L.-S. Tang, R.-Y. Bao, L. Bai, Z.-Y. Liu, B.-H. Xie, M.-B. Yang, W. Yang, Hybrid network structure of boron nitride and graphene oxide in shape-stabilized composite phase change materials with enhanced thermal conductivity and light-to-electric energy conversion capability, Solar Energy Materials and Solar Cells. 174 (2018) 56–64. https://doi.org/10.1016/j.solmat.2017.08.025.

[116] N. Barhemmati-Rajab, T. Mahadevan, J. Du, W. Zhao, Thermal transport properties enhancement of paraffin via encapsulation into boron nitride nanotube: a molecular dynamics study, MRS Communications. 10 (2020) 475–481. https://doi.org/10.1557/mrc.2020.49.

[117] H. Tafrishi, S. Sadeghzadeh, F. Molaei, H. Siavoshi, Investigating the effects of adding hybrid nanoparticles, graphene and boron nitride nanosheets, to octadecane on its thermal properties, RSC Advances. 10 (2020) 14785–14793. https://doi.org/10.1039/D0RA01847C.

[118] C. Lin, Z. Rao, Thermal conductivity enhancement of paraffin by adding boron nitride nanostructures: A molecular dynamics study, Applied Thermal Engineering. 110 (2017) 1411–1419. https://doi.org/10.1016/j.applthermaleng.2016.09.065.

[119] C. Liu, P. Hu, Z. Xu, X. Ma, Z. Rao, Experimental investigation on thermal properties of sodium acetate trihydrate based phase change materials for thermal energy storage, Thermochimica Acta. (2019). https://doi.org/10.1016/j.tca.2019.02.002.

[120] Y. Luan, M. Yang, Q. Ma, Y. Qi, H. Gao, Z. Wu, G. Wang, Introduction of an organic acid phase changing material into metal-organic frameworks and the study of its thermal properties, Journal of Materials Chemistry A. (2016). https://doi.org/10.1039/c6ta01676f.

[121] X. Chen, H. Gao, M. Yang, L. Xing, W. Dong, A. Li, H. Zheng, G. Wang, Smart integration of carbon quantum dots in metal-organic frameworks for fluorescence-functionalized phase change materials, Energy Storage Materials. 18 (2019) 349–355. https://doi.org/10.1016/j.ensm.2018.08.015.

[122] L. Chen, R. Zou, W. Xia, Z. Liu, Y. Shang, J. Zhu, Y. Wang, J. Lin, D. Xia, A. Cao, Electro- and Photodriven Phase Change Composites Based on Wax-Infiltrated Carbon Nanotube Sponges, ACS Nano. 6 (2012) 10884–10892. https://doi.org/10.1021/nn304310n.

[123] B. Mohammadi, F. Ranjbar, Y. Ajabshirchi, Exergoeconomic analysis and multi-objective optimization of a semi-solar greenhouse with experimental validation, Applied Thermal Engineering. 164 (2020) 114563. https://doi.org/10.1016/j.applthermaleng.2019.114563.

[124] R.J. Warzoha, A.S. Fleischer, Improved heat recovery from paraffin-based phase change materials due to the presence of percolating graphene networks, International Journal of Heat and Mass Transfer. 79 (2014) 314–323. https://doi.org/10.1016/j.ijheatmasstransfer.2014.08.009.

[125] H. Sun, Z. Xu, C. Gao, Multifunctional, Ultra-Flyweight, Synergistically Assembled Carbon Aerogels, Advanced Materials. 25 (2013) 2554–2560. https://doi.org/10.1002/adma.201204576.

[126] H. Babaei, P. Keblinski, J.M. Khodadadi, Thermal conductivity enhancement of paraffins by increasing the alignment of molecules through adding CNT/graphene, International Journal of Heat and Mass Transfer. 58 (2013) 209–216. https://doi.org/10.1016/j.ijheatmasstransfer.2012.11.013.

[127] J.F. Li, W. Lu, Y.B. Zeng, Z.P. Luo, Simultaneous enhancement of latent heat and thermal conductivity of docosane-based phase change material in the presence of spongy graphene, Solar Energy Materials and Solar Cells. 128 (2014) 48–51. https://doi.org/10.1016/j.solmat.2014.05.018.

[128] S. Wu, D. Zhu, X. Zhang, J. Huang, Preparation and melting/freezing characteristics of Cu/paraffin nanofluid as phase-change material (PCM), Energy and Fuels. (2010). https://doi.org/10.1021/ef9013967.

[129] S. Kim, L.T. Drzal, High latent heat storage and high thermal conductive phase change materials using exfoliated graphite nanoplatelets, Solar Energy Materials and Solar

Cells. 93 (2009) 136–142. https://doi.org/10.1016/j.solmat.2008.09.010.

[130] S. Shaikh, K. Lafdi, K. Hallinan, Carbon nanoadditives to enhance latent energy storage of phase change materials, Journal of Applied Physics. 103 (2008) 094302. https://doi.org/10.1063/1.2903538.

[131] R. Parameshwaran, R. Jayavel, S. Kalaiselvam, Study on thermal properties of organic ester phase-change material embedded with silver nanoparticles, Journal of Thermal Analysis and Calorimetry. (2013). https://doi.org/10.1007/s10973-013-3064-9.

[132] L. Fan, J.M.M. Khodadadi, Thermal conductivity enhancement of phase change materials for thermal energy storage: A review, Renewable and Sustainable Energy Reviews. 15 (2011) 24–46. https://doi.org/10.1016/j.rser.2010.08.007.

[133] Y. Lin, C. Zhu, G. Alva, G. Fang, Palmitic acid/polyvinyl butyral/expanded graphite composites as form-stable phase change materials for solar thermal energy storage, Applied Energy. 228 (2018) 1801–1809. https://doi.org/10.1016/j.apenergy.2018.07.068.

[134] D. Shin, D. Banerjee, Enhancement of specific heat capacity of high-temperature silica-nanofluids synthesized in alkali chloride salt eutectics for solar thermal-energy storage applications, International Journal of Heat and Mass Transfer. 54 (2011) 1064–1070. https://doi.org/10.1016/j.ijheatmasstransfer.2010.11.017.

[135] M. Chieruzzi, G.F. Cerritelli, A. Miliozzi, J.M. Kenny, Effect of nanoparticles on heat capacity of nanofluids based on molten salts as PCM for thermal energy storage., Nanoscale Research Letters. 8 (2013) 448. https://doi.org/10.1186/1556-276X-8-448.

[136] H. Mehling, L.F. Cabeza, Heat and cold storage with PCM, 2008.

[137] R.S. Feigelson, 50 Years of Progress in Crystal Growth, in: Journal of Crystal Growth, 2004. https://doi.org/10.1016/j.jcrysgro.2004.01.042.

[138] H. Reichert, O. Klein, H. Dosch, M. Denk, V. Honkimäki, T. Lippmann, G. Reiter, Observation of five-fold local symmetry in liquid lead., Nature. 408 (2000) 839–41. https://doi.org/10.1038/35048537.

[139] S.H. Oh, Y. Kauffmann, C. Scheu, W.D. Kaplan, M. Rühle, Ordered liquid aluminum at the interface with sapphire, Science. (2005). https://doi.org/10.1126/science.1118611.

[140] A.L. Greer, Supercool order, Nature Materials. 5 (2006) 13–14.

https://doi.org/10.1038/nmat1557.

[141] T.U. Schülli, R. Daudin, G. Renaud, A. Vaysset, O. Geaymond, A. Pasturel, Substrate-enhanced supercooling in AuSi eutectic droplets, Nature. 464 (2010) 1174–1177. https://doi.org/10.1038/nature08986.

[142] M. Faucheux, G. Muller, M. Havet, A. LeBail, Influence of surface roughness on the supercooling degree: Case of selected water/ethanol solutions frozen on aluminium surfaces, International Journal of Refrigeration. (2006). https://doi.org/10.1016/j.ijrefrig.2006.01.002.

[143] T. Adachi, D. Daudah, G. Tanaka, Effects of supercooling degree and specimen size on supercooling duration of erythritol, ISIJ International. (2014). https://doi.org/10.2355/isijinternational.54.2790.

[144] K. Nakano, Y. Masuda, H. Daiguji, Crystallization and melting behavior of erythritol in and around two-dimensional hexagonal mesoporous silica, Journal of Physical Chemistry C. (2015). https://doi.org/10.1021/jp510048g.

[145] C.A. Stan, G.F. Schneider, S.S. Shevkoplyas, M. Hashimoto, M. Ibanescu, B.J. Wiley, G.M. Whitesides, A microfluidic apparatus for the study of ice nucleation in supercooled water drops, Lab on a Chip. 9 (2009) 2293. https://doi.org/10.1039/b906198c.

[146] A. Safari, R. Saidur, F.A. Sulaiman, Y. Xu, J. Dong, A review on supercooling of Phase Change Materials in thermal energy storage systems, Renewable and Sustainable Energy Reviews. 70 (2017) 905–919. https://doi.org/10.1016/j.rser.2016.11.272.

[147] B. Sandnes, J. Rekstad, Supercooling salt hydrates: Stored enthalpy as a function of temperature, Solar Energy. 80 (2006) 616–625. https://doi.org/10.1016/j.solener.2004.11.014.

[148] E.P. Ona, X. Zhang, S. Ozawa, H. Matsuda, H. Kakiuchi, M. Yabe, M. Yamazaki, M. Sato, Influence of ultrasonic irradiation on the solidification behavior of erythritol as a PCM, Journal of Chemical Engineering of Japan. (2002). https://doi.org/10.1252/jcej.35.290.

[149] T. Shichiri, T. Nagata, Effect of electric currents on the nucleation of ice crystals in the melt, Journal of Crystal Growth. (1981). https://doi.org/10.1016/0022-0248(81)90461-

9.

[150] J.W. Mullin, K.D. Raven, Influence of mechanical agitation on the nucleation of some aqueous salt solutions, Nature. (1962). https://doi.org/10.1038/195035a0.

[151] M. Dalvi-Isfahan, N. Hamdami, E. Xanthakis, A. Le-Bail, Review on the control of ice nucleation by ultrasound waves, electric and magnetic fields, Journal of Food Engineering. 195 (2017) 222–234. https://doi.org/10.1016/j.jfoodeng.2016.10.001.

[152] A. Di Pretoro, F. Manenti, Crystallization, in: SpringerBriefs in Applied Sciences and Technology, 2020: pp. 109–114. https://doi.org/10.1007/978-3-030-34572-3_13.

[153] J. Mullin, Crystallization, 2001.

[154] M. Dannemand, J. Dragsted, J. Fan, J.B. Johansen, W. Kong, S. Furbo, Experimental investigations on prototype heat storage units utilizing stable supercooling of sodium acetate trihydrate mixtures, Applied Energy. (2016). https://doi.org/10.1016/j.apenergy.2016.02.038.

[155] M. Fashandi, S.N. Leung, Sodium acetate trihydrate-chitin nanowhisker nanocomposites with enhanced phase change performance for thermal energy storage, Solar Energy Materials and Solar Cells. (2018). https://doi.org/10.1016/j.solmat.2018.01.037.

[156] W. Cui, Y. Yuan, L. Sun, X. Cao, X. Yang, Experimental studies on the supercooling and melting/freezing characteristics of nano-copper/sodium acetate trihydrate composite phase change materials, Renewable Energy. (2016). https://doi.org/10.1016/j.renene.2016.08.001.

[157] Y. He, N. Zhang, Y. Yuan, X. Cao, L. Sun, Y. Song, Improvement of supercooling and thermal conductivity of the sodium acetate trihydrate for thermal energy storage with α-Fe2O3 as addictive, Journal of Thermal Analysis and Calorimetry. (2018). https://doi.org/10.1007/s10973-018-7166-2.

[158] J. Mao, J. Li, J. Li, G. Peng, A selection and optimization experimental study of additives to thermal energy storage material sodium acetate trihydrate, in: 2009 International Conference on Energy and Environment Technology, ICEET 2009, 2009. https://doi.org/10.1109/ICEET.2009.11.

[159] N. Beaupere, U. Soupremanien, L. Zalewski, Nucleation triggering methods in supercooled phase change materials (PCM), a review, Thermochimica Acta. (2018).

https://doi.org/10.1016/j.tca.2018.10.009.

[160] Q. Mei, J. Li, Dependence of liquid supercooling on liquid overheating levels of al small particles, Materials. (2016). https://doi.org/10.3390/ma9010007.

[161] P. Rudolph, H.J. Koh, N. Schäfer, T. Fukuda, The crystal perfection depends on the superheating of the mother phase too - Experimental facts and speculations on the "melt structure" of semiconductor compounds, Journal of Crystal Growth. (1996). https://doi.org/10.1016/0022-0248(96)00119-4.

[162] E.-B.B.S.B.S. Mettawee, G.M.R.R. Assassa, Thermal conductivity enhancement in a latent heat storage system, Solar Energy. 81 (2007) 839–845. https://doi.org/10.1016/j.solener.2006.11.009.

[163] A. García-Romero, G. Diarce, J. Ibarretxe, A. Urresti, J.M. Sala, Influence of the experimental conditions on the subcooling of Glauber's salt when used as PCM, Solar Energy Materials and Solar Cells. (2012). https://doi.org/10.1016/j.solmat.2012.03.003.

[164] H.W. Ryu, S.W. Woo, B.C. Shin, S.D. Kim, Prevention of supercooling and stabilization of inorganic salt hydrates as latent heat storage materials, Solar Energy Materials and Solar Cells. 27 (1992) 161–172. https://doi.org/10.1016/0927-0248(92)90117-8.

[165] N. Kumar, D. Banerjee, R. Chavez, Exploring additives for improving the reliability of zinc nitrate hexahydrate as a phase change material (PCM), Journal of Energy Storage. (2018). https://doi.org/10.1016/j.est.2018.09.005.

[166] Y. Dutil, D.R. Rousse, N. Ben Salah, S. Lassue, L. Zalewski, A review on phase-change materials: Mathematical modeling and simulations, Renewable and Sustainable Energy Reviews. 15 (2011) 112–130. https://doi.org/10.1016/j.rser.2010.06.011.

[167] A. Caggiano, C. Mankel, E. Koenders, Reviewing theoretical and numerical models for PCM-embedded cementitious composites, Buildings. 9 (2018). https://doi.org/10.3390/buildings9010003.

[168] D. Mazzeo, G. Oliveti, Parametric study and approximation of the exact analytical solution of the Stefan problem in a finite PCM layer in a steady periodic regime, International Communications in Heat and Mass Transfer. 84 (2017) 49–65. https://doi.org/10.1016/j.icheatmasstransfer.2017.03.013.

[169] V.R. Voller, J.B. Swenson, C. Paola, An analytical solution for a Stefan problem with variable latent heat, International Journal of Heat and Mass Transfer. 47 (2004) 5387–5390. https://doi.org/10.1016/j.ijheatmasstransfer.2004.07.007.

[170] P. Lamberg, Approximate analytical model for two-phase solidification problem in a finned phase-change material storage, Applied Energy. 77 (2004) 131–152. https://doi.org/10.1016/S0306-2619(03)00106-5.

[171] P.A. Mirzaei, F. Haghighat, Modeling of phase change materials for applications in whole building simulation, Renewable and Sustainable Energy Reviews. 16 (2012) 5355–5362. https://doi.org/10.1016/j.rser.2012.04.053.

[172] A. Sciacovelli, F. Colella, V. Verda, Melting of PCM in a thermal energy storage unit: Numerical investigation and effect of nanoparticle enhancement, International Journal of Energy Research. 37 (2013) 1610–1623. https://doi.org/10.1002/er.2974.

[173] V. Voller, M. Cross, Accurate solutions of moving boundary problems using the enthalpy method, International Journal of Heat and Mass Transfer. 24 (1981) 545–556. https://doi.org/10.1016/0017-9310(81)90062-4.

[174] P.H. Price, M.R. Slack, The effect of latent heat on numerical solutions of the heat flow equation, British Journal of Applied Physics. 5 (1954) 285–287. https://doi.org/10.1088/0508-3443/5/8/304.

[175] N.R. Eyres, D.R. Hartree, J. Ingham, R. Jackson, R.J. Sarjant, J.B. Wagstaff, The calculation of variable heat flow in solids, Philosophical Transactions of the Royal Society of London. Series A, Mathematical and Physical Sciences. 240 (1946) 1–57. https://doi.org/10.1098/rsta.1946.0002.

[176] M. Ainsworth, J.T. Oden, A Posteriori Error Estimation in Finite Element Analysis, John Wiley & Sons, Inc., Hoboken, NJ, USA, 2000. https://doi.org/10.1002/9781118032824.

[177] J. Mackenzie, W. Mekwi, On the use of moving mesh methods to solve PDEs., in: T. Tang, J. Xu (Eds.), Adaptive Computations, Theory and Algorithms, Science Press, Beijing, 2007: pp. 242–278.

[178] J.A. Mackenzie, M.L. Robertson, A Moving Mesh Method for the Solution of the One-Dimensional Phase-Field Equations, Journal of Computational Physics. 181 (2002) 526–544. https://doi.org/10.1006/jcph.2002.7140.

1736 [179] D.R. Lynch, K. O'Neill, Continuously deforming finite elements for the solution of
1737 parabolic problems, with and without phase change, International Journal for
1738 Numerical Methods in Engineering. 17 (1981) 81–96.
1739 https://doi.org/10.1002/nme.1620170107.
1740 [180] D.R. Lynch, Unified approach to simulation on deforming elements with application to
1741 phase change problems, Journal of Computational Physics. 47 (1982) 387–411.
1742 https://doi.org/10.1016/0021-9991(82)90090-0.
1743 [181] V.R. Voller, M. Cross, N.C. Markatos, An enthalpy method for convection/diffusion
1744 phase change, International Journal for Numerical Methods in Engineering. 24 (1987)
1745 271–284.
1746 [182] V.R. Voller, An implicit enthalpy solution for phase change problems: with application
1747 to a binary alloy solidification, Applied Mathematical Modelling. 11 (1987) 110–116.
1748 https://doi.org/10.1016/0307-904X(87)90154-5.
1749 [183] V.R. Voller, C.R. Swaminathan, B.G. Thomas, Fixed grid techniques for phase change
1750 problems: A review, International Journal for Numerical Methods in Engineering. 30
1751 (1990) 875–898. https://doi.org/10.1002/nme.1620300419.
1752 [184] M. Costa, D. Buddhi, a. Oliva, Numerical simulation of a latent heat thermal energy
1753 storage system with enhanced heat conduction, Energy Conversion and Management.
1754 39 (1998) 319–330. https://doi.org/10.1016/S0196-8904(96)00193-8.
1755 [185] A. Esen, S. Kutluay, A numerical solution of the Stefan problem with a Neumann-type
1756 boundary condition by enthalpy method, Applied Mathematics and Computation. 148
1757 (2004) 321–329. https://doi.org/10.1016/S0096-3003(02)00846-9.
1758 [186] N.R. Vyshak, G. Jilani, Numerical analysis of latent heat thermal energy storage
1759 system, Energy Conversion and Management. 48 (2007) 2161–2168.
1760 https://doi.org/10.1016/j.enconman.2006.12.013.
1761 [187] Y. Cao, A. Faghr, A numerical analysis of phase-change problems including natural
1762 convection, Journal of Heat Transfer. 112 (1990) 812–816.
1763 https://doi.org/10.1115/1.2910466.
1764 [188] S. Wang, A. Faghri, T.L. Bergman, A comprehensive numerical model for melting
1765 with natural convection, Int. J. Heat Mass Transf. 53 (n.d.) 1986–2000.
1766 [189] P. Damronglerd, Y. Zhang, Modified temperature-transforming model for convection-

controlled melting, Journal of Thermophysics and Heat Transfer. 21 (2007) 203–208. https://doi.org/10.2514/1.21529.

[190] Y. Cao, A. Faghri, Performance characteristics of a thermal energy storage module: a transient PCM/forced convection conjugate analysis, International Journal of Heat and Mass Transfer. 34 (1991) 93–101. https://doi.org/10.1016/0017-9310(91)90177-G.

[191] K.A.R. Ismail, C.T. Salinas, J.R. Henriquez, Comparison between PCM filled glass windows and absorbing gas filled windows, 40 (2008) 710–719. https://doi.org/10.1016/j.enbuild.2007.05.005.

[192] P.K. Goyal, A. Dutta, V. Verma, I. Thangamani, R. Singh, Enthalpy Porosity Method for CFD Simulation of Natural Convection Phenomenon for Phase Change Problems in the Molten Pool and its Importance during Melting of Solids, Undefined. (1986).

[193] C. Huber, A. Parmigiani, B. Chopard, M. Manga, O. Bachmann, Lattice Boltzmann model for melting with natural convection, International Journal of Heat and Fluid Flow. 29 (2008) 1469–1480. https://doi.org/10.1016/j.ijheatfluidflow.2008.05.002.

[194] E. alami Semma, M. El ganaoui, R. Bennacer, Lattice Boltzmann method for melting/solidification problems, C. R. Mecanique. 335 (2007) 295–303. https://doi.org/10.1016/j.crme.2007.05.015.

[195] D. Chatterjee, S. Chakraborty, An enthalpy-based lattice Boltzmann model for diffusion dominated solid-liquid phase transformation, Physics Letters, Section A: General, Atomic and Solid State Physics. 341 (2005) 320–330. https://doi.org/10.1016/j.physleta.2005.04.080.

[196] J. Miranda Fuentes, K. Johannes, F. Kuznik, M. Cosnier, J. Virgone, Melting with convection and radiation in a participating phase change material, Applied Energy. 109 (2013) 454–461. https://doi.org/10.1016/j.apenergy.2012.11.031.

[197] P.L. Bhatnagar, E.P. Gross, M. Krook, A model for collision processes in gases. I. Small amplitude processes in charged and neutral one-component systems, Physical Review. 94 (1954) 511–525. https://doi.org/10.1103/PhysRev.94.511.

[198] D. Chatterjee, 7 Lattice Boltzmann Modeling for Melting/Solidification Processes, n.d.

[199] C.Y.Y. Zhao, Y.B.B. Tao, Y.S.S. Yu, Molecular dynamics simulation of nanoparticle effect on melting enthalpy of paraffin phase change material, International Journal of Heat and Mass Transfer. 150 (2020) 119382.

https://doi.org/10.1016/j.ijheatmasstransfer.2020.119382.

[200] A.D. MacKerell, D. Bashford, M. Bellott, R.L. Dunbrack, J.D. Evanseck, M.J. Field, S. Fischer, J. Gao, H. Guo, S. Ha, D. Joseph-McCarthy, L. Kuchnir, K. Kuczera, F.T.K. Lau, C. Mattos, S. Michnick, T. Ngo, D.T. Nguyen, B. Prodhom, W.E. Reiher, B. Roux, M. Schlenkrich, J.C. Smith, R. Stote, J. Straub, M. Watanabe, J. Wiórkiewicz-Kuczera, D. Yin, M. Karplus, All-atom empirical potential for molecular modeling and dynamics studies of proteins, Journal of Physical Chemistry B. 102 (1998) 3586–3616. https://doi.org/10.1021/jp973084f.

[201] M. Sheikholeslami, A. Zareei, M. Jafaryar, A. Shafee, Heat transfer simulation during charging of nanoparticle enhanced PCM within a channel, Physica A. 525 (2019) 557–565. https://doi.org/10.1016/j.physa.2019.03.082.

[202] P. Di Giogio, M. Iasiello, A. Viglione, m. Mameli, S. Filippeschi, P. Di Marco, A. Andreozzi, N. Bianco, Numerical Analysis of a Paraffin/Metal Foam Composite for Thermal Storage , in: J. Phys.: Conf. Ser. 796 012032, 2017. https://doi.org/10.1088/1742-6596/796/1/012032.

[203] P. Atkin, M.M. Farid, Improving the efficiency of photovoltaic cells using PCM infused graphite and aluminium fins, Solar Energy. 114 (2015) 217–228. https://doi.org/10.1016/j.solener.2015.01.037.

[204] X. Hu, F. Zhu, X. Gong, Experimental and numerical study on the thermal behavior of phase change material infiltrated in low porosity metal foam, Journal of Energy Storage. 26 (2019) 101005. https://doi.org/10.1016/j.est.2019.101005.

[205] C. Wang, L. Feng, W. Li, J. Zheng, W. Tian, X. Li, Shape-stabilized phase change materials based on polyethylene glycol/porous carbon composite: The influence of the pore structure of the carbon materials, Solar Energy Materials and Solar Cells. 105 (2012) 21–26. https://doi.org/10.1016/j.solmat.2012.05.031.

[206] Z. Ling, J. Chen, T. Xu, X. Fang, X. Gao, Z. Zhang, Thermal conductivity of an organic phase change material/expanded graphite composite across the phase change temperature range and a novel thermal conductivity model, Energy Conversion and Management. 102 (2015) 202–208. https://doi.org/10.1016/j.enconman.2014.11.040.

[207] W. Li, Y. Dong, X. Zhang, X. Liu, Preparation and Performance Analysis of Graphite Additive/Paraffin Composite Phase Change Materials, Processes. 7 (2019) 447. https://doi.org/10.3390/pr7070447.

[208] Y.. Zhang, Y. Jiang, A simple method, the T-history method, of determining the heat of fusion, specific heat and thermal conductivity of phase-change materials, Measurement Science and Technology. 10 (1999). https://doi.org/https://doi.org/10.1088/0957-0233/10/3/015.